Mon. Not. R. Astron. Soc. **000**, 1–18 (2008) Printed 26 July 2010 (MN LATEX style file v2.2)

Grain sedimentation inside giant planet embryos.

Sergei Nayakshin
Department of Physics & Astronomy, University of Leicester, Leicester, LE1 7RH, UK

Accepted 2008 ?? ??. Received 2008 ?? ??; in original form 2008 05 ??

ABSTRACT

In the context of massive fragmenting protoplanetary discs, Boss (1998) suggested that grains can grow and sediment inside giant planet embryos formed at $R \sim 5$ AU away from the star. Several authors since then criticised the suggestion. Convection may prevent grain sedimentation, and the embryos cannot even form so close to the parent star as cooling is too inefficient at these distances. Here we reconsider the grain sedimentation process suggested by Boss (1998) but inside an embryo formed, as expected in the light of the cooling constraints, at $R \sim 100$ AU. Such embryos are much less dense and are also cooler. We make analytical estimates of the process and also perform simple spherically symmetric radiation hydrodynamics simulations to test these ideas. We find that convection in our models does not become important before a somewhat massive ($\sim$ an Earth mass, this is clarified in a followup paper) solid core is built. Turbulent mixing slows down dust sedimentation but is overwhelmed by grain sedimentation when the latter grow to a centimetres size. The minimum time required for dust sedimentation to occur is a few thousand years, and is a strong function of the embryo's mass, dust content and opacity. An approximate analytical criterion is given to delineate conditions in which a giant embryo contracts and heats up faster than dust can sediment. As Boss et al. (2002), we argue that core formation through grain sedimentation inside the giant planet embryos may yield an unexplored route to form giant gas and giant ice planets. The present model also stands at the basis of paper III, where we study the possibility of forming terrestrial planet cores by tidal disruption and photoevaporation of the planetary envelope.

Key words:

1 INTRODUCTION

The Gravitational Instability (GI) model for giant planet formation (e.g., Bodenheimer 1974; Boss 1997) is one of the two well known models for planet formation (e.g., Wetherill 1990). The model has been thought to be unable to produce solid cores observed in giant planets in the Solar System (e.g., Fortney & Nettelmann 2009) until Boss (1998); Boss et al. (2002) demonstrated that dust growth and sedimentation may realistically occur inside gaseous protoplanets. However, Wuchterl et al. (2000) argued that giant planet embryos may become convective within the first $\sim$ 100 years of their evolution, and that convection may inhibit grain sedimentation. Helled et al. (2008); Helled & Schubert (2008) have recently confirmed that convection may indeed be a serious obstacle to solid core formation inside the giant planet embryos. These authors obtained much smaller cores than the model of Boss (1998) predicts. More recently, the GI model for giant planet formation has been criticised on the grounds that the cooling time at the inner, e.g., $R \lesssim 10$ AU disc, is not short enough to permit a continuous gravitational contraction of gaseous clumps (e.g., Rafikov 2005; Rice et al. 2005).

Whilst this criticism of Boss (1998) ideas appears to be relevant, there are now extrasolar giant planets observed at distances out to hundreds of AU from their parent star, where the core accretion model (e.g., Weidenschilling 1980; Wetherill 1990) for planet formation may not have been able to create solid cores before the gaseous disc dissipates. It seems rather likely that the GI model is needed to explain these planets. Simulations of large (e.g., tens of AU) discs that employ realistic cooling in the optically thick regime do show formation of gaseous clumps with masses of a few to a few tens of Jupiter masses (e.g., Stamatellos & Whitworth 2008; Meru & Bate 2010), which presumably cool and contract into giant planets or brown dwarfs.

It is timely to reconsider the gravitational disc instability model taking into account the updated constraints on the disc fragmentation (e.g., Rafikov 2005). To investigate this complicated and non-linear problem properly, we divide presentation of our work into several papers – (1, this paper) before and (2, Nayakshin 2010b, to be submitted) after the solid core formation, and (3, Nayakshin 2010c, submitted to

MNRAS letters) interplay of the processes occurring inside the embryo with external influences of the parent disc and the star.

The goal of this paper (referred in later papers as "paper I") is to study dust growth and sedimentation inside the giant embryo but excluding the solid core formation. We limit our study to isolated non-rotating giant planet embryos or first cores, the terms that we use inter-exchangeably below. While the study of such a limited problem may appear too academical, we shall use these results extensively in papers II and III. There is also a possibility that dust sedimentation inside first cores may also be relevant to the process of low mass star formation. Therefore we hope that analytical results presented here may be useful for future researchers in more than one field.

The gist of the "new" disc fragmentation constraints is that the giant planet embryo must start off much less dense than previously assumed. Namely, Boss (1998) assumed that the protoplanet has a mean density of order $\sim 10^{-8}$ g cm^{-3}. Such high a density is needed to overcome the tidal fields from the parent star at several AU distances. However, at $\sim$ 100 AU, the initial embryo density of order $\sim 10^{-13}$ g cm^{-3} is expected (see paper II for detail). Optical depths of such embryos are much less than of those studied by Boss (1998); Wuchterl et al. (2000); Helled et al. (2008). Therefore we find that the giant planet embryo remains radiative long enough to permit dust growth and sedimentation. In fact, convection becomes important only after the solid core assembly as the energy release by the solid core rises to as much as $10^{28} - 10^{29}$erg s^{-1} (paper II).

The paper is organised as following. In §2, we introduce the so-called "first cores" and argue that the initial state of giant planet embryos should be similar to that of the first cores. In §3 we study the internal evolution of *isolated* first cores, defining the maximum gas accretion rate onto the first core under which the core can be considered isolated. We then attempt to carry out the calculations analytically as far as we can, building a simple analytical model to follow the cooling and contraction of the first cores, and grain growth and sedimentation inside them. We also consider the influence of turbulent mixing and grain shattering via high speed collisions that may delay the onset of grain sedimentation.

In later parts of the paper, §4 and §5, we use a simple spherically symmetric radiation hydrodynamics code with a two-fluid approach to capture grain growth and dynamics to allow for a simultaneous evolution of the gas and the dust. We find higher opacity, larger metalicity and lower mass first cores to be the most promising sites of grain sedimentation. Turbulent mixing mainly slows down rather than forbids grain sedimentation; although in corners of the parameter space it may be crucially important. We conclude that whether the grains sediment inside the first core or not mainly depends on whether it contracts and hence heats to the grain vaporisation temperature faster than the grains can grow. Finally, in the Discussion section we overview the main results of our work, compare those to previous work, and consider implications for the field of planet formation. We argue that the planet formation community should take a detailed look at the giant instability disc model supplemented by a realistic internal evolution for the giant embryo, and also embryo dynamics in the parent disc.

2 FIRST CORES AND GIANT PLANET EMBRYOS

2.1 First cores in studies of star formation

Stars form from larger gas reservoirs due to gravitational contraction of the latter. The simplest case of a spherical, uniform, non-rotating, and initially at rest, constant density cloud is well known (Larson 1969). The collapsing gas is initially isothermal, as cooling is very effective. However, as the innermost region of the collapsing gas fragment becomes denser, the free fall time there becomes shorter than the cooling time of the gas (Masunaga & Inutsuka 1999). The region switches from an isothermal to an adiabatic behaviour. Heated up, the gas is able to stop the further collapse by thermal pressure forces. The central part of the region settles into a hydrostatic balance. This region is logically named "the first core".

The minimum mass of the first cores is given by the "opacity limit" (Rees 1976; Low & Lynden-Bell 1976) of a few Jupiter masses (although Masunaga & Inutsuka 1999, note that the term is somewhat physically misleading), and the size is $\sim 10^{14}$ cm. The conditions in a typical *non rotating* Solar mass molecular gas cloud puts the first cores in a situation where the mass supply rate is continuous and relatively high ($\sim$ a few $\times 10^{-5}\,$M$_\odot$ yr^{-1}). In this case new matter lands on the first core so fast that it does not have time to cool, and therefore the behaviour of the gas nearly adiabatic (Larson 1969; Masunaga et al. 1998; Masunaga & Inutsuka 2000). They contract and heat up only due to more and more mass piling up on them from the parent gas cloud. When their mass exceeds about 50 Jupiter masses, the cores reach the temperature of about $2000K$ and the gas density about 10^{-8} g cm^{-3}. Dissociation of molecular hydrogen then ensues. This provides an additional energy sink and initiates a "second collapse" which finally turns the first core into a true proto-star as compact as a few Solar radii.

To understand why the first cores do not collapse further until they reach a mass of about $M_{\rm max} = 0.05\,$M$_\odot$ (Masunaga et al. 1998; Masunaga & Inutsuka 2000), consider the virial temperature of the first core. As will be shown latter (equation 12), an adiabatically evolving first core has the virial temperature of about

$$T_{\rm vir} = \frac{GM_{\rm fc}\mu}{3k_B R_{\rm fc}} \sim 150\ {\rm K}\ \left(\frac{M_{\rm fc}}{0.01\,{\rm M}_\odot}\right)^{4/3}\ , \qquad (1)$$

where $M_{\rm fc}$ and $R_{\rm fc}$ are the mass and the radius of the first core, respectively. The core becomes hot enough for hydrogen to disassociate only when it reaches the mass of about 50 Jupiter masses.

2.2 Giant planet embryos are similar to first cores

Consider now the properties of giant planet embryos at the moment of their formation in a protoplanetary disc. In order to fragment gravitationally, a massive gas disc must satisfy two criteria. First of all, it must be massive/dense enough. In particular, the Toomre (1964) Q-parameter must be less than unity:

$$Q = \frac{c_s \Omega}{\pi G \Sigma} \leqslant 1\ , \qquad (2)$$

where c_s is the gas isothermal sound speed; $\Omega = (GM_*/R_p^3)^{1/2}$ is Kepler's angular frequency; M_* is the mass of the star, assumed to be larger than that of the disc, and $\Sigma = 2H\rho$ is the surface density of the disc. Here ρ is the disc vertically averaged density, and $H = c_s\Omega^{-1}$ is the disc vertical scale-height. Rearranging equation 2, we see that at $Q = 1$ the disc mean density is equal to the tidal density of the star,

$$\rho_{\rm t} = \frac{M_*}{2\pi R_p^3} \approx 10^{-13}\ {\rm g\ cm^{-3}}\ \frac{M}{\rm M_\odot} R_2^{-2}\ , \quad (3)$$

to within a factor of order unity, where $R_2 = R_p/100$ AU.

The second condition for disc fragmentation is the condition on the rate of cooling. Expressed in terms of the cooling time $t_{\rm cool}$, the requirement states (Gammie 2001; Rice et al. 2005):

$$t_{\rm cool} \lesssim 3\Omega^{-1}\ . \quad (4)$$

This implies that the critical radiative cooling rate per unit gram of disc material is

$$\Lambda_{\rm crit} = \frac{e}{t_{\rm cool}} \approx \frac{c_s^2\Omega}{3(\gamma-1)}\ , \quad (5)$$

where γ is the specific heats ratio for gas. At the same time, the compressional heating rate for gravitational contraction is (Masunaga & Inutsuka 1999)

$$\Lambda_{\rm grav} = c_s^2\,(4\pi G\rho)^{1/2} = 2^{1/2}\ c_s^2\Omega\ , \quad (6)$$

where we have used equation 3 to eliminate ρ. It is now clear that $\Lambda_{\rm crit} \approx \Lambda_{\rm grav}$ at the point of disc fragmentation[1]. This is intuitively correct, as otherwise the disc could heat up faster than it could fragment, increasing c_s and returning itself back to stability (e.g., $Q > 1$).

We have shown above that a fragmenting self-gravitating gas disc satisfies $\Lambda_{\rm crit} \approx \Lambda_{\rm grav}$. This is also the condition that sets the "opacity limit for fragmentation" in star formation (Rees 1976; Low & Lynden-Bell 1976; Masunaga et al. 1998; Masunaga & Inutsuka 1999), which yields a minimum mass for fragmentation of a few Jupiter masses. This is of course not a coincidence as in both cases gravitational collapse is stopped if the gas is unable to continue cooling rapidly enough.

Therefore the properties of the gaseous clumps in the disc at their inception should be similar to that of the first cores of a few Jupiter masses. As with the first cores, the clumps may gain more mass from the disc. However, the giant planet embryos in the disc have to compete for gas with other embryos, as the disc is likely to fragment on many rather than one clump. Collisions between clumps may unbind the clumps partially or completely. Furthermore, it is well known that above the "transition" mass $M_t \approx 2M_*(H/R)^3$ (Bate et al. 2003) the planet opens up a gap in the disc due to gravitational torques between the planet and the disc, and that the gap opening curtails gas accretion onto the planet by orders of magnitude (Lubow et al. 1999; Bate et al. 2003). Giant planet embryos with mass of the order of 10 Jupiter masses are in this gap-opening regime as long as $H/R \lesssim 0.2$ for a Solar mass star.

Therefore, for simplicity, we study the evolution of planet embryos at a constant mass in this paper. The mass of the gaseous clump is a free parameter below. We also use the terms "first core" and "giant planet embryo" interexchangeably throughout.

[1] This statement is accurate within a factor of order unity, e.g., the same order of accuracy to which the vertically integrated accretion disc equations (Shakura & Sunyaev 1973) are to be trusted.

3 INTERNAL EVOLUTION OF FIRST CORES

3.1 Physical properties of adiabatic first cores

Masunaga et al. (1998) show that the structure of the first cores can be well approximated by a polytropic sphere, with the polytropic constant fixed by the gas temperature and the density $\rho_{\rm ad}$ at which the gas switches from the isothermal to the adiabatic behaviour. The typical values of these are often taken in the literature as $T_{\rm init} = 10$ K and $\rho_{\rm ad} = 10^{-13}$ g cm^{-3}. However, $\rho_{\rm ad}$ does depend on the opacity of the material and the ambient gas temperature $T_{\rm init}$ (Masunaga & Inutsuka 1999). Following these authors, we take opacity to be dominated by dust, in the functional form

$$\kappa(T) = \kappa_0 \left(\frac{T}{10}\right)^\alpha\ , \quad (7)$$

where κ_0 is the opacity at $T = 10$ K, and reasonable values of α are thought to be between 1 and 2. With this, the adiabatic density threshold is best described by the following (Masunaga & Inutsuka 1999):

$$\rho_{\rm ad} = 5\times10^{-13}\kappa_*^{-2/3}T_1^{\frac{4-2\alpha}{3}}\ {\rm g\ cm^{-3}}\ , \quad (8)$$

where $\kappa_* = \kappa_0/0.01$ and $T_1 = T_{\rm init}/10$K.

Masunaga et al. (1998) give expression for $R_{\rm fc}$ as a function of the central density. Eliminating the density in favour of the sphere's mass and radius, we obtain

$$R_{\rm fc} = 17.5\ {\rm AU}\ m_1^{-1/3}T_1\rho_{-13}^{-2/3}\ , \quad (9)$$

where $\rho_{-13} = 10^{13}\rho_{\rm ad}$, $T_1 = T_{\rm init}/10$ and $m_1 = M_{\rm fc}/0.01\ {\rm M_\odot}$. Eliminating the critical density by using equation 8, we get

$$R_{\rm fc} = 6.0\ {\rm AU}\ m_1^{-1/3}T_1^{\frac{1+4\alpha}{9}}\kappa_*^{4/9}\ . \quad (10)$$

Note that the temperature dependence in this expression is at most linear, and the opacity enters in an even weaker power. The initial size of the first core is hence varies rather little. The mean density of the first core is defined by

$$\rho_{\rm mean} = \frac{3M_{\rm fc}}{4\pi R_{\rm fc}^3} = 6.6\times10^{-12}\ {\rm g\ cm^{-3}}\ m_1^2T_1^{-\frac{1+4\alpha}{3}}\kappa_*^{-4/3}\ , \quad (11)$$

and is a very strong function of the mass of the first core. The temperature of the first core is of the order of the virial temperature, which we estimate to be

$$T_{\rm vir} = \frac{1}{3}\frac{GM_{\rm fc}\mu}{k_BR_{\rm fc}} = 146\ {\rm K}\ m_1^{4/3}T_1^{-\frac{1+4\alpha}{9}}\kappa_*^{-4/9}\ . \quad (12)$$

From this it follows that the sound speed in the first core is, $c_s = \sqrt{kT/\mu} \approx \sqrt{GM_{\rm fc}/R_{\rm fc}}$,

$$c_s = 0.7\ {\rm km\ s^{-1}}\ m_1^{2/3}T_1^{-\frac{1+4\alpha}{18}}\kappa_*^{-2/9} \quad (13)$$

The column depth of the first core is

$$\Sigma_{\rm fc} = \frac{M_{\rm fc}}{\pi R_{\rm fc}^2} = 1.18\times 10^3 \ {\rm g\ cm^{-2}}\ m_1^{5/3} T_1^{\frac{2+8\alpha}{9}} \kappa_*^{-8/9} \ , \quad (14)$$

and the optical depth of the first core is

$$\tau_{\rm core} = \kappa(T_{\rm vir})\Sigma_{\rm fc} = 11.8\times (14.6)^{\alpha} m_1^{\frac{5+4\alpha}{3}} \phi_1(T_1,k_*) \ , \quad (15)$$

where $\phi_1(T_1,\kappa_*) = T_1^{\frac{2+7\alpha-4\alpha^2}{9}} \kappa_*^{\frac{1-4\alpha}{9}}$. From this expression it is obvious that the first cores are always optically thick. The radiative luminosity of the first core is

$$L_{\rm fc} \approx \frac{4\pi R_{\rm fc}^2 \sigma_B T_{\rm vir}^4}{\kappa \Sigma_{\rm fc}} \ , \quad (16)$$

or numerically,

$$L_{\rm fc} = 2.2\times 10^{32} (14.6)^{-\alpha} m_1^{\frac{9-4\alpha}{3}} \phi_2(T_1,\kappa_*) \ , \quad (17)$$

where function $\phi_2(T_1,\kappa_*) = T_1^{(4-15\alpha+4\alpha^2)/9}\ \kappa_*^{-1+4\alpha/9}$ is a cumbersome looking power-law function which does not vary much for α between 1 and 2, however. For example, for $\alpha = 1$, $\phi_2(T_1,\kappa_*) = T_1^{7/9}\kappa_*^{-5/9}$, whereas for $\alpha = 2$, $\phi_2(T_1,\kappa_*) = T_1^{10/9}\kappa_*^{-1/9}$. Nevertheless, it does become quite inconvenient to write down expressions for a general value of α, and so we shall present the results only for either $\alpha = 1$ or $\alpha = 2$ below. For convenience of future reference,

$$L_{\rm fc} = \begin{cases} 1.5\times 10^{31} m_1^{5/3} T_1^{7/9} k_*^{-5/9} & \text{for } \alpha = 1 \\ 1.0\times 10^{30} m_1^{1/3} T_1^{10/9} k_*^{-1/9} & \text{for } \alpha = 2\ . \end{cases} \quad (18)$$

Note that the luminosity is lower for $\alpha = 2$ than for the other case. This is due to a higher opacity of the first core, e.g., the larger exponent in the opacity law. The binding energy of the polytropic sphere,

$$E_{\rm bind} = \frac{3}{5}\frac{GM_{\rm fc}^2}{R_{\rm fc}} = 1.8\times 10^{41}\ {\rm erg}\ m_1^{7/3} T_1^{-\frac{1+4\alpha}{9}} \kappa_*^{-4/9} \ , \quad (19)$$

allows us to calculate the cooling time of the sphere as

$$t_{\rm cool} = \frac{E_{\rm bind}}{L_{\rm fc}} \ . \quad (20)$$

For the smaller value, $\alpha = 1$,

$$t_{\rm cool} = 380\ {\rm years}\ m_1^{2/3} T_1^{-4/3} \kappa_*^{1/9} \ , \quad (21)$$

whereas for $\alpha = 2$,

$$t_{\rm cool} = 5700\ {\rm years}\ m_1^{2} T_1^{-19/9} \kappa_*^{-1/3} \ . \quad (22)$$

Another useful time scale is the dynamical time of the core, which is of the order of the free fall time for the core:

$$t_{\rm dyn} = (G\rho_{\rm mean})^{-1/2} \approx 50\ {\rm yrs}\ m_1^{-1} T_1^{\frac{1+4\alpha}{6}} \kappa_*^{2/3} \quad (23)$$

Note that the cooling time is indeed longer than dynamical time, as should be for a hydrostatic gas configuration.

3.2 Gas-starved regime for the first cores

Having reviewed the adiabatic evolution of the first cores, we can now estimate when cooling of the cores becomes important. As the core gains (or perhaps looses mass), the adiabatic temperature time derivative is

$$\left(\frac{dT_{\rm vir}}{dt}\right)_{\rm ad} = \frac{\partial T_{\rm vir}}{\partial M_{\rm fc}}\frac{dM_{\rm fc}}{dt} = \frac{4}{3}\ T_{\rm vir}\frac{d\ln M_{\rm fc}}{dt} \ , \quad (24)$$

where we used equation 12. On the other hand, the temperature derivative due to radiative cooling is

$$\left(\frac{dT_{\rm vir}}{dt}\right)_{\rm rad} = \frac{T_{\rm vir}}{t_{\rm cool}} \quad (25)$$

(see also equation 29 below). We define a critical "radiative" first core accretion or decretion rate as the one for which $|(dT_{\rm vir}/dt)_{\rm rad}| = (dT_{\rm vir}/dt)_{\rm ad}$. For mass gain or loss rate below this critical rate, the radiative cooling is the dominant driver of the cloud's thermal evolution. From equation 25 and 24 we find

$$\left|\frac{dM_{\rm fc}}{dt}\right|_{\rm rad} = \frac{3M_{\rm fc}}{4t_{\rm cool}} = \quad (26)$$

$$= \begin{cases} 2\times 10^{-5}\ {\rm M_\odot yr^{-1}}\ m_1^{1/3} T_1^{4/3} k_*^{-1/9} & \text{for } \alpha = 1 \\ 1.3\times 10^{-6}\ {\rm M_\odot yr^{-1}}\ m_1^{-1} T_1^{19/9} k_*^{1/3} & \text{for } \alpha = 2 \end{cases} \quad (27)$$

Note further that as the first cores contract, their cooling time $t_{\rm cool}$ increases (§3.3 below), and hence the critical radiative accretion rate actually drops with time from the value found in equation 27.

We can now compare the critical radiative accretion rates with the accretion rates of the first cores in the context of a Solar mass gas cloud collapsing, for which the first cores accumulate mass at the rate $dM_{\rm fc}/dt \sim 10^{-5}\ {\rm M_\odot\ yr^{-1}}$ (Larson 1969; Masunaga et al. 1998; Masunaga & Inutsuka 2000). These rates are higher than the critical radiative accretion rates, and therefore the first cores should indeed evolve quasi-adiabatically in these conditions.

In the opposite case, $|dM_{\rm fc}/dt| \ll (dM_{\rm fc}/dt)_{\rm rad}$, the evolution of the first cores will be governed mainly by their radiative cooling. This is the case that we henceforth study in this paper.

3.3 Cooling of isolated cores

Staying within the analytical approach, we calculate the cooling evolution of the first cores, assuming that they remain polytropic spheres. The solutions obtained in this way will be later compared to a numerical calculation that does not use this assumption.

We obtain the solution by solving the equation $dE_{\rm bind}/dt = L_{\rm fc}$, where the plus sign is used because we defined the binding energy to be positive. For convenience, we introduce dimensionless temperature $\tilde{T}(t)$ of the first core as the ratio of the current virial temperature $T(t)$ to the initial virial temperature of the core at formation, as given by equation 12. We also introduce a constant for a given $M_{\rm fc}$, $t_0 = t_{\rm cool}(0)$, which is the cooling time of the first core at formation, given by equation 20.

Equation 16 shows that luminosity of the first core changes with time as

$$L_{\rm fc} \propto R_{\rm fc}^4 T^{4-\alpha} \propto \tilde{T}^{-\alpha} \ ; \quad (28)$$

where we used the fact that $R_{\rm fc}T \propto$ is a constant for a given $M_{\rm fc}$. Since the binding energy scales as $E_{\rm bind} \propto T(t)$ at a fixed $M_{\rm fc}$, the equation for the evolution of the dimensionless temperature of the first core can be written as

$$\frac{d\tilde{T}}{dt} = \frac{\tilde{T}^{-\alpha}}{t_0} \ , \quad (29)$$

which is solved as

$$\tilde{T}(t) = \left[1 + (1+\alpha)\ \frac{t}{t_0}\right]^{\frac{1}{1+\alpha}} \ . \quad (30)$$

Using this, we find for the cooling time evolution

$$t_{\rm cool}(t) = t_{\rm cool}(0) + (1+\alpha)t \ , \tag{31}$$

which in the limit $t \gg t_{\rm cool}(0)$ shows that the cooling time is always $1+\alpha$ times the current time. Note that this implies that the first core's cooling becomes more inefficient as it contracts. The luminosity of the core evolves according to

$$L_{\rm fc}(t) = L_{\rm fc}(0)\left[1 + (1+\alpha)\,\frac{t}{t_0}\right]^{\frac{\alpha}{1+\alpha}} \ , \tag{32}$$

where $L_{\rm fc}(0)$ is the initial luminosity of the core, given by equation 18. Note that equation 32 is an increasing function of time, so that the first cores do become brighter as they contract, but the binding energy of the core increases with t even faster, and this is why the cooling time is a growing function of time as well.

We can now define the time scale $t_{\rm vap}$ defined as the time needed for the first core to heat up to the temperature $T_{\rm vap}$ at which grains vaporise (see §4.2.2; $T_{\rm vap} \sim 1200 - 1400K$, depending on the size of the grains). This time scale is obtained by solving

$$T_{\rm vap} = T_{\rm vir}\left[1 + (1+\alpha)\,\frac{t_{\rm vap}}{t_0}\right]^{\frac{1}{1+\alpha}} \ , \tag{33}$$

where $T_{\rm vir}$ is the initial virial temperature of the first core as given by equation 12. As an example, in the limiting cases when $t_{\rm vap} \gg t_0$, the results are:

$$t_{\rm vap} = 1.3\times10^4 \text{ years } \left(\frac{T_{\rm vap}}{1200\,\rm K}\right)^2 m_1^{-2} T_1^{-2/9} \kappa_* \ , \tag{34}$$

for $\alpha = 1$, and

$$t_{\rm vap} = 1.6\times10^6 \text{ years } \left(\frac{T_{\rm vap}}{1200\,\rm K}\right)^3 m_1^{-2} T_1^{8/9} \kappa_* \tag{35}$$

for $\alpha = 2$. These time scales are very long, and are strongly dependent on the mass of the first core. The term neglected in the last two equations becomes important for more massive cores that are already hot at their birth. They may reach the vaporisation temperature very quickly.

Figure 1 shows the evolution of the virial temperature (simply referred to as temperature of the first cores hereafter) for several values of $M_{\rm fc}$ as a function of time for the two limiting opacity cases. The curves are computed using equation 30. The upper panel presents the faster contracting case $\alpha = 1$ and the lower one corresponds to $\alpha = 2$. In the case of the lower opacity ($\alpha = 1$), the relatively massive cores, $M_{\rm fc} \gtrsim 20 M_J$, contract quite rapidly during the first few thousand years. In terms of grain growth and sedimentation, these cores are not very promising, as we shall see below. In contrast, for $M_{\rm fc} \lesssim 10 M_J$ for $\alpha = 1$, and for all values of $M_{\rm fc}$ for $\alpha = 2$, the cores take $t > 10^4 - 10^5$ years to contract to the grain vaporisation temperature. Grain growth is plausible in these cases.

We also plot first core's mean densities as a function of time in Figure 2. As in Figure 1, the curves are terminated when the core's temperature rises above $1400K$, as then the grains would be vaporised. We see that the lower mass first cores evolve (contract) significantly before vaporisation of grains occur. This again hints at less massive first cores as the more promising sites of grain growth and sedimentation, as they simply stay cooler for longer.

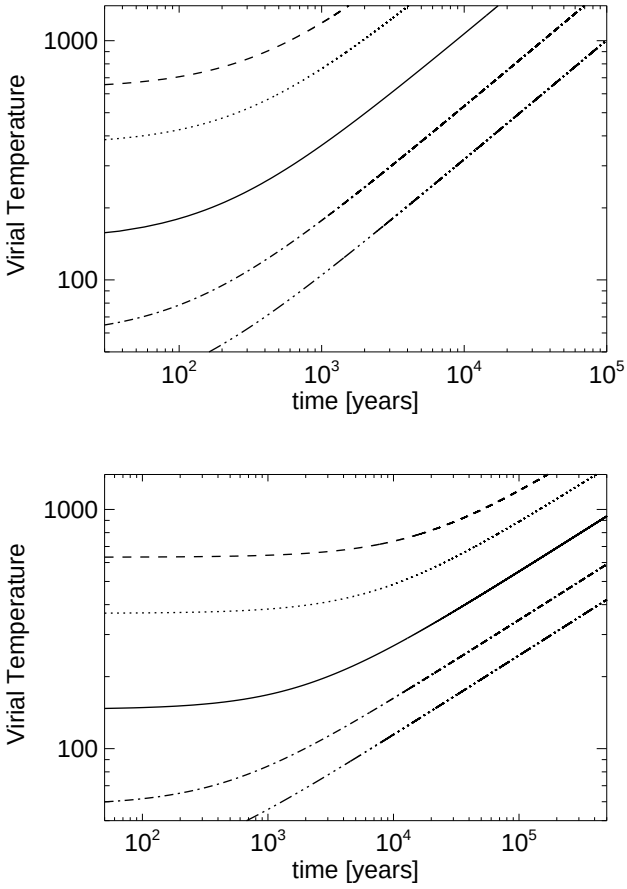

Figure 1. Virial temperature as a function of time in the analytical model for cores of different masses, $M_{\rm fc} = 3, 5, 10, 20$ and $30\ M_J$, from bottom to top curves, respectively. The **top** panel is for opacity power-law index $\alpha = 1$, whereas the **bottom** panel is for $\alpha = 2$. The plots are terminated at $T = 1400$ K, when even the largest grains would vaporise rapidly. Note that lower mass cores could support grain growth for longer as they are initially cooler.

3.4 Time scales for grain growth and sedimentation

Boss (1998) studied formation of gaseous giant planets by gravitational instability in a proto-planetary disc. He considered a gaseous clump that would eventually contract to form a proto-planet of mass $M = 1 M_J$. Boss (1998) demonstrated that if the conventional arguments for dust growth and sedimentation are specialised for the spherical geometry of the clump, then one can expect a rather rapid dust growth and sedimentation which may culminate in a formation of a heavy elements core.

Because of the specifics of the gravitational disc instability model for planet formation, the gas density of 10^{-8} g cm^{-3} was used for the gaseous clump. As shown in §3.1, our gaseous clumps are much less dense and are also cooler in their initial stages. Nevertheless, the line of arguments of Boss (1998) for the dust growth and sedimentation model can be simply rescaled to the problem at hand. Our treatment thus follows his model.

We shall first assume that turbulent motions in the first

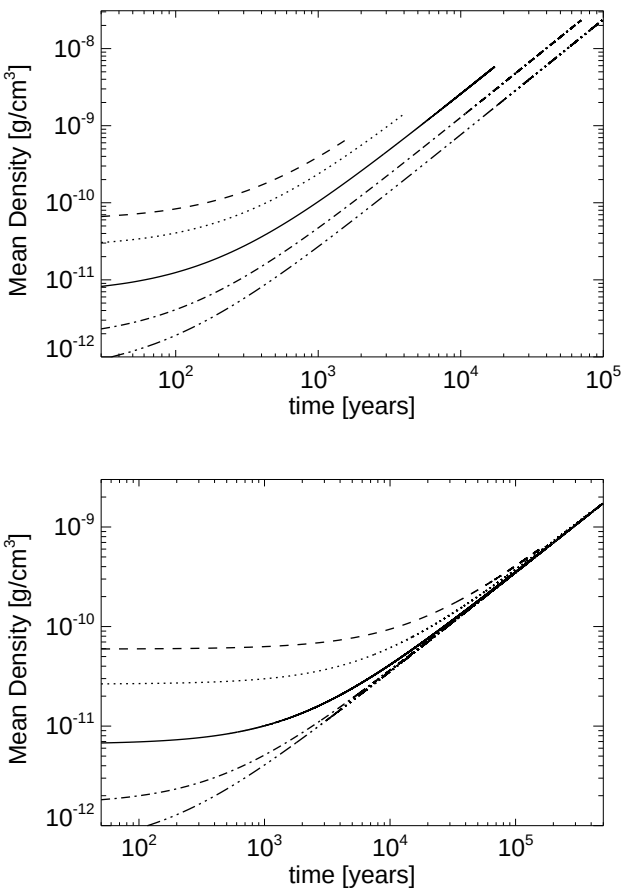

Figure 2. Same as in Figure 1, but now showing the mean density of the first cores. The mean density curves are terminated when first core's temperature reaches $T = 1400$ K. Note that maximum mean densities are a few $\times 10^{-10}$ g cm^{-3} for the more massive cores but can reach $\sim 10^{-8}$ g cm^{-3} for the least massive cores.

core can be neglected. This allows us to make the most optimistic estimates of grain growth and sedimentation. The importance of turbulence will be elaborated in §3.7, and further tested with numerical models in §3.

Further, we note that realistically, grains of different sizes are present in the cloud at any given time, due to fragmentation of larger grains by high speed collisions. Only a fraction of grains is large enough to start sedimenting down. Therefore the mass fraction f_g in our model should be thought to represent only those larger grains. A sizable fraction of the original grains is assumed to remain small and tightly bound to the gas. Accordingly, a constant gas opacity of the form given by equation 7 is used despite allowing larger grains to sediment.

Following Safronov (1969); Weidenschilling (1980); Boss (1998), we assume that the grains can grow by the hit-and-stick mechanism (but see Blum & Wurm 2008). For a constant density core, the gravitational acceleration, $a_{\rm gr}$,

$$a_{\rm gr} = -\frac{4\pi}{3} G \rho_{\rm fc} R \, , \tag{36}$$

where $R \leqslant R_{\rm fc}$ is the radial position of the grain inside the first core.

There is no pressure gradient force for the grains, but there is a gas-grain drag force if the grain velocity, u_a, is different from that of gas, u. Note that u_a is always subsonic with respect to the gas speed of sound, as the largest velocity that the grain can attain is the free-fall velocity which is of the same order as c_s by definition.

The drag force on a spherical body depends on the Reynolds number, $Re = a|\Delta u|/\lambda c_s$, where $\Delta u = u_a - u$, and λ is the mean free path for hydrogen molecules in the gas. The latter is relatively large, e.g., $\lambda = 1/(n\sigma_{\rm H2}) \approx 40$ cm ρ_{-10}^{-1}, where $\rho_{-10} = 10^{10}\rho_{\rm fc}$ is the dimensionless density of the first core. As we shall see below, grains will usually satisfy $a \lesssim \lambda$, in which case the Epstein drag law applies, and one has (Boss 1998)

$$\left(\frac{du_a}{dt}\right)_{\rm drag} = -\frac{\rho_{\rm fc} c_s}{\Sigma_a}(u_a - u) \, . \tag{37}$$

Here a, $\Sigma_a = \rho_a a$ and $\rho_a \sim 1$ g cm^{-3} are the radius, the column and the mass density of the grain, respectively.

For a larger body, $a > \lambda$, the Stokes drag law applies. The law also depends on the relative velocity Δu through the Reynolds number (see Weidenschilling 1977). In the limit of the small $Re < 1$, The Stokes law yields

$$\left(\frac{du_a}{dt}\right)_{\rm drag} = -\frac{3\rho_{\rm fc} c_s}{2\Sigma_a}\frac{\lambda}{a}\,(u_a - u) \, . \tag{38}$$

Neglecting the complicated behaviour of the drag coefficient for intermediate values of Re, we combine both regimes described by equations 37 and 38 into one, approximately, as

$$\left(\frac{du_a}{dt}\right)_{\rm drag} = -\frac{\rho_{\rm fc} c_s}{\Sigma_a}\frac{\lambda}{a+\lambda}(u_a - u) \, . \tag{39}$$

Given our simple one size dust model, a better gas drag treatment appears to be excessive, but future more detailed calculations should utilise more careful drag force treatments.

The equation of motion for the grain is then

$$\frac{du_a}{dt} = -\frac{\rho_{\rm fc} c_s}{\Sigma_a}\frac{\lambda}{a+\lambda}(u_a - u) - \frac{4\pi}{3} G \rho_{\rm fc} R \, . \tag{40}$$

Small grains, $a \ll \rho_{\rm fc} R/\rho_a$, quickly reach their terminal velocity, so that $du_a/dt \approx 0$, and the grains slip through the gas in the direction of the centre of the cloud with the sedimentation velocity

$$-u_{\rm sed} = (u_a - u) = -\frac{4\pi G \Sigma_a R}{3 c_s}\,\frac{\lambda + a}{\lambda} \, . \tag{41}$$

Note that this velocity is proportional to R. For this reason, for a given radius of the grain a, grains starting at different R will fall to the centre at the same time. We refer to this time scale as the sedimentation or dust settling time:

$$t_{\rm sed} = \frac{R}{u_{\rm sed}} \approx \frac{3 c_s}{4\pi G \Sigma_a}\frac{\lambda}{a+\lambda} \approx 5{\times}10^3 \text{ yrs } m_1^{2/3}(\rho_a a)^{-1} \, , \tag{42}$$

where the density of the grain ρ_a and its size a are in cgs units, and we assumed $a \ll \lambda$ limit in the last step.

For microscopic grains, say 1 micron, the sedimentation time scale is prohibitively long. Therefore grains must become larger before any sedimentation takes place. The early growth of microscopic grains is dominated by Brownian motions of the smallest grains (Dullemond & Dominik 2005). Since the sedimentation velocity is a function of the grain

size a, grains of different size move with differential speeds. Hence the larger grains sweep smaller grains, leading to the growth of the grain's mass, $m_a = (4\pi/3)\rho_a a^3$, at the rate

$$\frac{dm_a}{dt} = \pi a^2 f_g \rho u_{\rm sed} \ , \tag{43}$$

where $f_g = 0.01$ is the mass fraction of grains, so that $\rho_g = f_g\rho$ is the density of grain material. This translates into the growth rate for a of

$$\frac{da}{dt} = \frac{f_g\rho}{4\rho_a} u_{\rm sed} \ . \tag{44}$$

One finds that this differential settling grain growth is faster than that due to Brownian motion for larger grains. We now define the grain size e-folding time scale, $t_{\rm e} = a/(da/dt)$,

$$t_{\rm e}(0) = \frac{3c_s}{\pi f_g \rho_{\rm fc} G R} \ . \tag{45}$$

Using $R \sim R_{\rm fc}$, the grain growth time scale is defined as the time needed to increase the grain size from an initial value a_0 to the final size a:

$$t_{\rm gr} = \frac{3c_s}{\pi f_g \rho_{\rm fc} G R_{\rm fc}} \ \ln\frac{a}{a_0} \ . \tag{46}$$

Choosing $a = 10$ cm and $a_0 = 10^{-4}$ cm as an example, $\ln(a/a_0) \approx 23$. Noting that $R_{\rm fc}/c_s = t_{\rm dyn} \sim (G\rho)^{-1/2}$, we see that for $f_g = 0.01$, some 2×10^3 dynamical times need to pass before the grains attain a size at which they can sediment rapidly. Using the relations from §3.1, we have

$$t_{\rm gr}(0) = 5.4 \times 10^4 m_1^{-1} f_{-2}^{-1} k_*^{2/3} T_1^{-(5+20\alpha)/18} \frac{\ln(a/a_0)}{20} \ , \tag{47}$$

in years, where $f_{-2} = f_g/0.01$. In this equation we emphasised the fact that the grain growth time estimate is obtained for $t = 0$.

3.5 Time-dependent grain growth

Comparing the grain growth time scale with the cooling times of the first cores (equations 21 and 22), and with the longer vaporisation times (equations 34 and 35), one is tempted to think that grain growth is too slow to be of importance, especially for the lower opacity index, $\alpha = 1$. However one needs to be more careful here as the first core contracts with time. Therefore grain growth actually accelerates as the gas cloud cools, and especially rapidly for the case $\alpha = 1$.

Using equation 46 and our model for the evolution of the first cores, we plot the time-dependent estimate for the grain growth time scale in Figure 3 for the same first core masses as in Figures 1 and 2. Although the lower mass cases (upper curves in Figure 3) initially have longer grain growth time scales, they are also initially cooler and stay sufficiently cool to avoid the second collapse for longer. Therefore, these cores should be promising sites of grain growth after a few hundred years, when they cross the line shown with diamonds, which is simply the current time.

We can improve the analytical estimate for the time needed for grain growth (equation 47) by utilising the results from §3.3. We observe that $t_{\rm gr} \propto c_s/(\rho_{\rm fc} R_{\rm fc}) \propto (M_{\rm fc}/R_{\rm fc})^{1/2}(R_{\rm fc}^2/M_{\rm fc}) \propto \tilde{T}(t)^{-3/2}$ at a constant $M_{\rm fc}$. Therefore, the equation for the grain growth in a contracting first core is

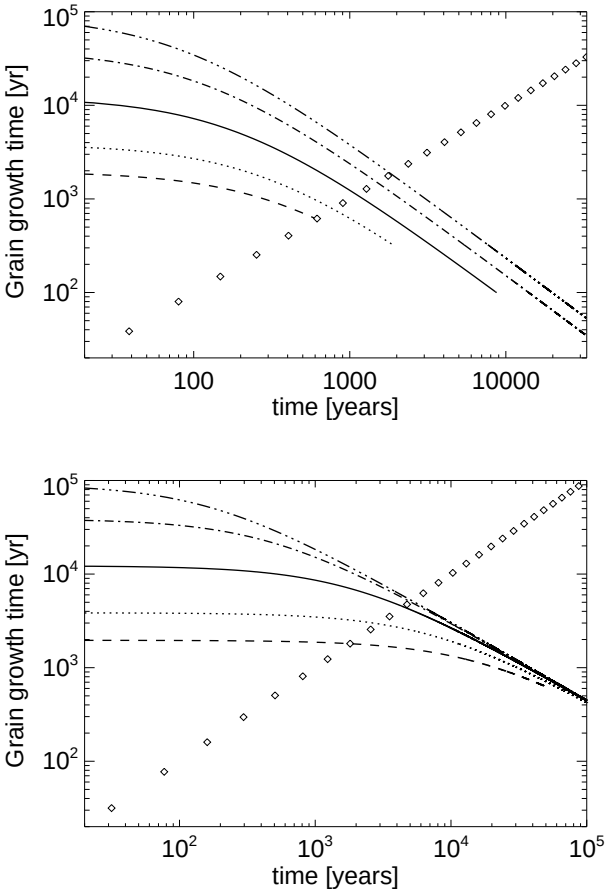

Figure 3. Grain growth time scale, $t_{\rm gr}$ (equation 46), for time-evolving first cores of different masses and the two opacity cases (cf. Figures 1 and 2). The diamonds show the line $t_{\rm gr} = t$. Anywhere where the $t_{\rm gr}$ curve drops below the diamond line, the grain growth is possible. The curves are terminated when the cores become hot enough to vaporise the grains. Lower opacity ($\alpha = 1$) and higher mass first cores cannot support substantial grain growth and sedimentation.

$$\frac{da}{dt} = \frac{a}{t_{\rm e}(0)} \left[1 + (1+\alpha)\,\frac{t}{t_0}\right]^{\frac{1.5}{1+\alpha}} \ . \tag{48}$$

This equation can be integrated analytically, and inverted to give a more accurate estimate for the grain growth time from size a_0 to a:

$$t_{\rm gr} = \frac{t_0}{1+\alpha} \ \left[\left(1 + \frac{2.5+\alpha}{t_0} t_{\rm gr}(0)\right)^{\xi} - 1\right] \ , \tag{49}$$

where $\xi = (1+\alpha)/(2.5+\alpha)$. In practically all the interesting parameter space, $t_{\rm gr}(0) \gg t_0$, and the above equation can be further simplified to

$$t_{\rm gr} = \frac{(2.5+\alpha)^{\xi}}{1+\alpha} t_0^{1-\xi} t_{\rm gr}(0)^{\xi} \ . \tag{50}$$

This results in considerably shorter grain growth times. In particular, for $\alpha = 1$, omitting the dependence on T_1,

$$t_{\rm gr}(a) = 3.3 \times 10^3 m_1^{-2/7} f_{-2}^{-4/7} k_*^{9/21} \left(\frac{\ln(a/a_0)}{20}\right)^{4/7} \ , \tag{51}$$

and for $\alpha = 2$,

$$t_{\rm gr}(a) = 2.3\times 10^4 f_{-2}^{-2/3} k_*^{1/3} \left(\frac{\ln(a/a_0)}{20}\right)^{2/3} . \quad (52)$$

Both of these cases show that grain growth is possible within a reasonable range of parameters, as the vaporisation time $t_{\rm vap}$ can be comfortably longer than this. Furthermore, numerical experiments (§4) show that grain growth time is about a factor of two shorter than the analytical model predicts.

3.6 Sedimentation for a constant grain size

Based on our numerical experiments below, grains do not sediment strongly until their size reaches at least a few cm. Approximately then, we divide the process of grain growth and sedimentation into the growth phase, studied above, and the sedimentation phase. Assuming that grain growth slows down in the latter phase (due, e.g., to a too high relative velocity between the grains, see §3.8), we consider the grains to have a constant size whilst they sediment. This simplified model allows analytical calculations to be carried through. We shall continue to approximate the first core with the constant density $\rho = \rho_{\rm fc}$ for $R \leqslant R_{\rm fc}$ and zero density outside, as in §3.1. Furthermore, we shall fix these, essentially assuming that sedimentation occurs on a time scale shorter than the current cooling time of the first core.

3.6.1 Homologous contraction in the gas-dominated phase

We start off with the grain density radial distribution following the gas distribution, thus $\rho_g(R,0) = f_g\rho_{\rm fc}$, and zero grain velocity. The gas is assumed stationary. One can show that the grains achieve the terminal velocity $u = -u_{\rm sed}$ (equation 41) very quickly when $|v_a| \ll c_s$. Here we kept the dependence of the drag force on the grain size in the more general form (equation 39). Note that the sedimentation time scale $t_{\rm sed}$ is independent of R in the limit $a \ll \lambda$ (see equation 42). Radial position of grains evolves according to

$$\frac{dR}{dt} = -\frac{R}{t_{\rm sed}} , \quad (53)$$

which is trivially solved,

$$R(t) = R_0 \exp\left[-\frac{t}{t_{\rm sed}}\right] , \quad (54)$$

where R_0 is the initial value of R. $R(t)$ is the Lagrangian coordinate for a grain mass shell $M_g(R_0)$. This equation shows that the grains contract homologously, so that the grain density is independent of radius within $R_{\rm g}(t) = R_{\rm fc}\exp(-t/t_{\rm sed})$, and is zero outside. The grain density profile keeps its top-hat shape but becomes more compact. The grain density increases with time as

$$\rho_g(t) = f_g\rho_{\rm fc}\exp\left[\frac{3t}{t_{\rm sed}}\right] . \quad (55)$$

3.6.2 Grain-dominated core phase

The equation 41 for the grain settling velocity neglects gravity from grains, which is appropriate in the initial stages of the process. When the density of the grains approaches and then exceeds that of the gas, the equation obviously becomes inaccurate. The contracting cloud of grains becomes self-gravitating at the time

$$t_{\rm self} = t_{\rm sed}\frac{\ln(f_g^{-1})}{3} = 1.53\ t_{\rm sed} . \quad (56)$$

The grain sphere's outermost radius at that time is

$$R_{\rm self} = R_{\rm fc} f_g^{1/3} \approx 0.2\left[\frac{f_g}{0.01}\right]^{1/3} R_{\rm fc} . \quad (57)$$

Thus to follow the contraction of the grain sphere after time $t_{\rm self}$, we modify the equation for settling velocity by writing

$$\frac{dR}{dt} = -\frac{GM_g(R_0)}{R^2}\frac{\Sigma_a(a+\lambda)}{\rho_{\rm fc}\lambda c_s} , \quad (58)$$

which now completely neglects the mass of the gas interior to radius R, as $\rho_g \gg \rho_{\rm fc}$, asymptotically. Since $M_g(R) = M_g(R_0)$, i.e., constant in Lagrangian coordinates, the above equation is solved as

$$R(t) = R(t_{\rm self})\left[1 - 3\,\frac{t-t_{\rm self}}{t_{\rm sed}}\right]^{1/3} , \quad (59)$$

which is a homologous contraction again, albeit at a different – accelerated by the self-gravity – rate. The density evolution follows the form

$$\rho_g(t) = \rho_{\rm fc}\left[1 - 3\,\frac{t-t_{\rm self}}{t_{\rm sed}}\right]^{-1} , \quad (60)$$

where we utilised the fact that the grain density at the initial time when the solution 60 becomes applicable, $t = t_{\rm sed}$ is equal to $\rho_{\rm fc}$. Within this simple model, all the grains collect to the centre of the first core, reaching formally infinite densities, at time

$$t_\infty = t_{\rm self} + \frac{t_{\rm sed}}{3} = \frac{\ln(e/f_g)}{3}\ t_{\rm sed} = 1.87\ t_{\rm sed} \quad (61)$$

for $f_g = 0.01$.

3.6.3 Bound "grain cluster" phase

Before contraction of the grains into a point occurs, another important milestone is reached when the grain sphere becomes not only self-gravitating but also gravitationally self-bound. In the self-contracting phase studied above, the gravitational force acting on the grains is dominated by the grain density. Hence the grains are self-gravitating in that sense. However, if the outer gaseous envelope were removed in the beginning of that phase, gas inside the grain sphere would create a significant pressure gradient that could unbind the contracting grain-gas mix. In contrast, at later time, when the grain sphere contracts even further, its density is high enough that removal of the gaseous envelope would not unbind the grains. We refer to this stage as the "grain cluster" one, in analogy to a star cluster.

Consider then the question of how compact the grain sphere of mass $f_g M_{\rm fc}$ should be in order to be self-bound, i.e., so that the gas pressure could not unbind the sphere. We follow the usual order of magnitude arguments with which the Jean's mass can be derived. The gas pressure gradient is $\sim \rho k_B T/\mu R$, whereas the gravitational acceleration is $(GM_{\rm enc}(R)/R^2)(\rho+\rho_g)$. The total enclosed mass is $M_{\rm enc}(R) = (4\pi/3)(\rho+\rho_g)R^3$. This defines the radial scale (Jean's length and also the size of the grain cluster)

$$R_{\rm gc} = \left[\frac{3}{4\pi}\frac{k_B T}{\mu G}\frac{\rho}{\rho_g^2}\right]^{1/2} , \quad (62)$$

where we explicitly assumed $\rho \ll \rho_g$. The Jeans mass is equal to $M_J = M_{\rm gc} = (4\pi/3)\rho_g R_{\rm gc}^3$, which can be re-written as

$$M_{\rm gc} \approx \left(\frac{3}{4\pi\rho}\right)^{1/2}\left(\frac{k_B T}{\mu G}\right)^{3/2}\left(\frac{\rho}{\rho_g}\right)^2 . \quad (63)$$

The first two factors on the right hand side of the equation 63 is the mass of the first core, $M_{\rm fc}$. Further, $M_{\rm gc} = f_g M_{\rm fc}$, and hence we can solve for the grain density in the grain cluster:

$$\rho_{\rm gc} \approx \rho_{\rm fc}\, f_g^{-1/2} . \quad (64)$$

Using this result in equation 62, the radius of the grain cluster is found to be

$$R_{\rm gc} \approx R_{\rm fc}\, f_g^{1/2} = 0.1 R_{\rm fc}\left[\frac{f_g}{0.01}\right]^{1/2} . \quad (65)$$

This equation shows that the grain sphere becomes self-bound when it contracts to size $0.1R_{\rm fc}$, e.g., $0.1 - 1$ AU for a realistic range on parameters.

Note that the grain density in the grain cluster is typically a factor of ten or more higher than the density of the first core itself, i.e., as high as $10^{-9} - 10^{-7}$ g cm^{-3}.

Presumably, once the "grain cluster" phase is reached, nothing keeps the grain-dominated region from a self-gravitational collapse, so that a solid core could be formed (Boss 1998). We delay the study of this issue till a future paper.

3.7 Turbulent mixing

Turbulent mixing (Fromang & Papaloizou 2006) is a process in which grains are dragged along turbulent motions of the gas. As initially grains represent a small fraction of the total mass, they are essentially a trace population, and therefore gas turbulence drives diffusion of grains. This process hence tends to erase grain density inhomogeneities, opposing gravitational settling of the grains.

Numerical simulations (Fromang & Papaloizou (2006), and references thereafter) show that a simple diffusion equation approach describes the effects of turbulence on dust well, provided that the diffusion coefficient, D, is chosen right. The diffusion equation for grains in the spherical geometry can be written as

$$\frac{\partial \rho_g}{\partial t} = \frac{D}{R^2}\frac{\partial}{\partial R}\left[R^2\rho\frac{\partial(\rho_g/\rho)}{\partial R}\right] , \quad (66)$$

where ρ and ρ_g are the gas and the grain (dust) density, respectively. Note that we assumed that D is a constant inside the giant embryo, e.g., independent of R. The diffusion coefficient in case of disc can be parameterised in the form $D = \alpha_d c_s H$, reminiscent of the standard disc viscosity prescription (Shakura & Sunyaev 1973), where $\alpha_d < 1$ is the viscosity coefficient, and H is the disc vertical scale height. We shall use the same approach, except that the scale-height H should be replaced by the radius of the first core, $R_{\rm fc}$:

$$D = \alpha_d c_s R_{\rm fc} . \quad (67)$$

The diffusion coefficient α_d is unknown here. In the disc geometry, differential rotation velocity develops between the dust layer and the gas, driving instabilities (see, e.g., Garaud & Lin 2004). The simulations of the turbulent disc by Fromang & Papaloizou (2006) showed that $\alpha_d \sim 0.004$, but there is no clear reason why their results should translate to the case we study. Therefore we shall treat α_d as a free parameter of the model and consider the implications of turbulent diffusion in the "small" and "large" α_d cases.

To continue with our analytical modelling for now, we shall again assume the "top hat" density profile for the gas, and hence set ρ to a constant. Also, we shall combine the diffusion equation for dust (grains) with the mass continuity equation:

$$\frac{\partial \rho_g}{\partial t} = \frac{D}{R^2}\frac{\partial}{\partial R}\left[R^2\frac{\partial \rho_g}{\partial R}\right] - \frac{1}{R^2}\frac{\partial}{\partial R}\left[R^2\rho_g V\right] , \quad (68)$$

where $V = -u_{\rm sed}$ is the grain terminal velocity derived earlier (equation 41).

In a steady state, the solution of this equation implies

$$\rho_{\rm eq} = \rho_{d0}\exp\left[-\frac{R^2}{H_d^2}\right] , \quad (69)$$

where H_d is the "dust sphere" scale height, given by

$$H_d = (2Dt_{\rm sed})^{1/2} \quad (70)$$

Using equation 42 for sedimentation time $t_{\rm sed}$ and $c_s^2 = GM_{\rm fc}/R_{\rm fc}$, we obtain

$$\frac{H_d}{R_{\rm fc}} = \left[\frac{3\alpha_d}{2}\frac{\Sigma_{\rm fc}}{\Sigma_a}\frac{\lambda}{\lambda + a}\right]^{1/2} \quad (71)$$

where $\Sigma_{\rm fc} = M_{\rm fc}/(\pi R_{\rm fc}^2) \sim 10^3$ g cm^{-2} is the column depth of gas in the first core (equation 14). Recalling that $\Sigma_a = \rho_a a$, we see that for any grain sedimentation to take place (i.e., to have $H_d \ll R_{\rm fc}$), we need α_d to be small and a to be large, e.g., macroscopic. For example, if $\alpha_d = 0.001$, $a < \lambda$, and $\rho_a \sim 1$ g cm^{-3}, grains larger than 1 cm are required.

3.8 Destructive collisions

Experiments show that the simple hit-and-stick picture for grain growth is modified when the relative velocity is larger than a few metres per second (Blum & Wurm 2008). Above these speeds grains can fragment or stick only partially. Further growth-reducing processes such as cratering or partial fragmentation can occur. To estimate the potential importance of this, we recall that the terminal velocity of a grain of size a is

$$u_{\rm sed} = \frac{4\pi G\Sigma_a R}{3c_s} = 4.4\ {\rm m\ s^{-1}}\ a\ \frac{R}{R_{\rm fc}}\tilde{T}(t)^{-3/2} , \quad (72)$$

where $a \ll \lambda$ is in cm, and we assumed $M_{\rm fc} = 0.01\,{\rm M}_\odot$. Here the time-dependent dimensionless function $\tilde{T}(t)$ (equation 30) accounts for the fact that the first cores contract with time, so that $R_{\rm fc}/c_s \propto \rho_{\rm fc}(t)^{-1/2} \propto T(t)^{-3/2}$.

From the above equation we see that growth of cm-sized grains may stall as their sedimentation velocity exceeds several metres per second. For a qualitative estimate of the effects of this, we can further assume that grain growth saturates at a size a such that $u_{\rm sed} = v_{\rm max}$, where $v_{\rm max}$ is a few metres per second. In this case the grain sedimentation time scale is modified to

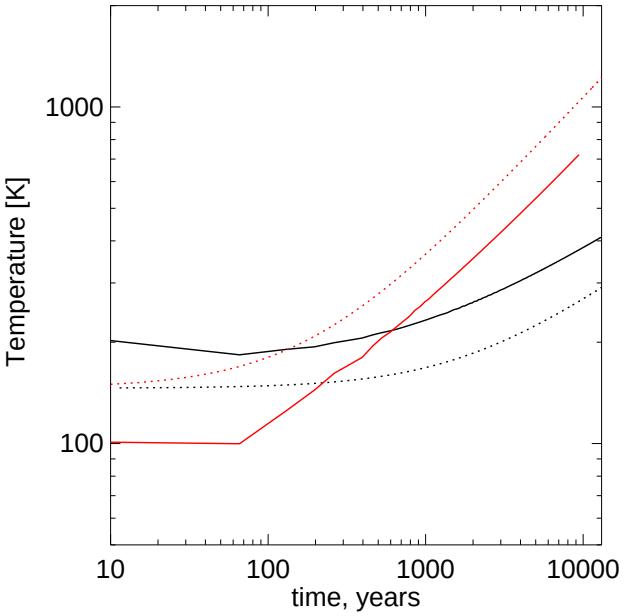

Figure 4. Mean temperature (solid curves) of the first core of mass $M_{\rm fc} = 10 M_J$ as a function of time for $\alpha = 1$ (red) and $\alpha = 2$ (black). The dotted curves show the virial temperature of the first cores in the analytical model presented in §3.3 for same cases. Note that the analytical curves are within $\sim 20-30\%$ of the numerical calculation.

$$t_{\rm fragm} = R_{\rm fc}/v_{\rm max} = 3\times 10^4 \ {\rm yr} \ \frac{R_{\rm fc}}{3\times 10^{13}} \frac{3 \, {\rm m \ s^{-1}}}{v_{\rm max}} \ . \quad (73)$$

This "fragmentation-limited" sedimentation is slow, but not prohibitively slow compared with the grain growth time and the vaporisation times calculated earlier. The qualitative indication is hence that fragmentation of grains may slow down but not stop grain sedimentation inside the first cores.

4 SET UP OF NUMERICAL MODELS

Having learned about the problem perhaps as much as possible within a simple analytical approach, we now turn to a spherically symmetric radiation hydrodynamics code to follow the evolution of the first cores and grain sedimentation inside them. We use Lagrangian (gas) mass coordinates and the classical radiative diffusion approximation, which is appropriate given that first cores are very optically thick except for their atmospheres, which are of little interest to us here.

4.1 No grain sedimentation case: gas only equations

First of all we shall present evolution of the first core neglecting dust growth and sedimentation. Besides being interesting in itself, such a calculation is useful to contrast with the analytical solutions we obtained in §3.3. The equations being solved are the standard hydrodynamical equation with the addition of the radiative diffusion cooling:

$$\frac{du}{dt} = -4\pi R^2 \frac{dP}{dM} - \frac{GM_{\rm tot}(R)}{R^2} + a_{\rm g-d} \ , \quad (74)$$

$$\frac{d\varepsilon}{dt} = -4\pi P \frac{d(R^2 u)}{dM} - 4\pi \frac{d(R^2 F_{\rm rad})}{dM} \ , \quad (75)$$

$$\frac{dR}{dt} = u \ , \quad (76)$$

where u is gas velocity, $M_{\rm tot}(R) = M(R) + M_g(R)$ is the total (gas + grains) mass enclosed within R, $a_{\rm g-d}$ is the acceleration due to the gas-dust drag, to be discussed below, P is gas pressure, $F_{\rm rad}$ is the classical radiation flux, given by

$$F_{\rm rad} = -\frac{4 a_{\rm rad} c T^3}{3\kappa(T)} 4\pi R^2 \frac{dT}{dM} \ , \quad (77)$$

where $a_{\rm rad}$ is the radiation constant. The gas density is defined by $\rho^{-1} = 4\pi R^2 dR/dM$. The numerical time integration procedure is based on the Lagrangian scheme "lh1" presented in Bodenheimer et al. (2007). The scheme uses artificial viscosity to capture shocks. We initialise the first cores as polytropic spheres of a given gas mass $M_{\rm fc}$ as described in §3.1.

Most of the simulations here do not include the convective energy transfer since we did not expect it to be important: the optical depth of the first cores is not very high, so radiative cooling is quite efficient until the gas clump contracts significantly. This was confirmed in some of the simulations that did include the convective energy transfer. Furthermore, all of the simulations in paper II include the convective flux, and also the resulting convective mixing of the grains. We found that convection is never dominant before the collapse of the central grain concentration into a massive solid core. Once that occurs, the release of gravitational energy from the core significantly changes the entropy profile near the solid core. This change drives very strong, in fact supersonic, convective motions in the region near the core. This strongly affects grain dynamics but *after* the solid core has already formed.

The boundary conditions at $R = 0$ are $u = 0$, $M(0) = 0$, $dP/dM = 0$ and $F_{\rm rad} = 0$. At the outer boundary we require continuity of gas density, velocity and the radiation flux. In this section we consider the case of dust tightly bound to the gas, in which case one can simply neglect the dust, setting $a_{\rm g-d}$ to zero.

Figure 4 shows the mean temperature in the cloud as a function of time for the first core of mass $M_{\rm fc} = 0.01 M_{\rm fc}$ for the two opacity cases, $\alpha = 1$ and $\alpha = 2$. The dimensionless opacity coefficient $k_* = 1$ and the ambient gas temperature $T_1 = 1$ for all the curves in the figure. The slight jumps in the solid curves are due to initial oscillations of the first cores, which quickly decay away due to artificial viscosity (the numerical representation of the polytropic sphere initial conditions results in small perturbations). We also plot the analytical solutions (dotted lines) for the same clouds and opacity cases as obtained in §3.3. Notably, the analytical and numerical solutions do not deviate from each other by more than a few tens of percent, which is more than can be expected from the order of magnitude analytical approach.

4.2 Inclusion of grain physics

4.2.1 Grain dynamics

We now turn our attention to the more complex case in which grain dynamics is taken into account. We use grains of the same size a for the whole cloud, where a is a free parameter. A more complex treatment is possible but is delayed until a future paper.

The grains are treated as a second fluid. We use the Lagrangian radial mesh provided by the gas coordinate to follow the evolution of dust. This is natural especially for small size grains that are strongly bound to the gas, as the relative gas-grain velocity is small, and the grains essentially move with the gas. The dust is described by a density in a given radial gas shell, and is allowed to slip through gas shells (see below). The grain initial density distribution follows that of gas, scaled down by the factor f_g.

The drag force acting on the grains/dust due to friction with the gas, $(du_a/dt)_{\rm drag}$, is given by equation 39. Due to Newton's second law, the back reaction on the gas is

$$\rho \left(\frac{du}{dt}\right)_{\rm drag} = -\rho_g \left(\frac{du_a}{dt}\right)_{\rm drag} , \quad (78)$$

where u_a is grain velocity, ρ_g is dust density (not to be confused with grain material density, ρ_a), and u is gas velocity. Accordingly, the acceleration $a_{\rm g-d}$ in equation 75 is simply $(du/dt)_{\rm drag}$.

The grains themselves are under the influence of gravity, drag force from the gas, and also undergo turbulent diffusion. From equation 68, this can be accounted for by setting the grain velocity to

$$u_a = u - u'_{\rm sed} - D\frac{\partial \ln(\rho_g/\rho)}{\partial R} \quad (79)$$

where $u'_{\rm sed}$ is the grain sedimentation velocity, and the last term is the grain velocity generated by turbulent mixing. The terminal velocity approach that is used to derive equation 79 is sufficiently accurate for small grains. For larger grains, the sedimentation velocity (equation 41) may be larger than the local free fall velocity. To correct for this, we use

$$u'_{\rm sed} = \min\left[u_{\rm sed}, u_{\rm ff}\right] , \quad (80)$$

where $u_{\rm ff} = \sqrt{2GM_{\rm tot}(R)/r}$ is the local free fall velocity. We tested this approach against the exact integration of grain radial time-dependent equation of motion, i.e., not assuming a terminal velocity. The differences are minor, and the terminal velocity approach is more numerically stable for smaller grains and does not require excessively small time steps. Therefore we pick the equation 79 as the superior approach for grain dynamics simulations here.

Note that mass $M_g(R)$, initially exactly equal to $f_g M(R)$, evolves with time separately from $M(R)$, as grains are allowed to slip through the gas, and from one gas radial mass shell into another. The mass continuity equation for grains inside a gas mass shell of index i, with inner and outer radii of R_i and R_{i+1}, respectively, is

$$\frac{1}{4\pi}\frac{\partial \Delta M_{g,i}}{\partial t} = -\left[R^2\rho_g(u_a-u)\right]_{i+1} + \left[R^2\rho_g(u_a-u)\right]_i , \quad (81)$$

where indeces $i+1$ and i refer to the inner and outer boundary of the zone; e.g., $\rho_{g,i}$ is density of dust in zone i, $\Delta M_{g,i} = (4\pi/3)\rho_{d,i}(R^3_{i+1} - R^3_i)$ is the grain mass inside zone i.

There is a slight uncertainty in choosing the boundary conditions for grains at $R \to 0$ radius, that is in the very first *gas* mass zone. In contrast to the gaseous component, grains are not supported by pressure effects there, thus they can sediment and form a phase *below* even the very first mass zone of the gas. On the other hand, turbulence may suspend the grains in the fluid, curtailing the sedimentation into $R = 0$. Our goal here is to be conservative in our calculations of grain sedimentation. Therefore we assume that the turbulence keeps the grains suspended in the very first gas zone *as long as* the gas dominates the grains there by mass. Accordingly, the boundary condition for grain velocity is set to $u_a(R = 0) = 0$, as for the gas, for all the numerical tests below. The simulations are stopped when the grain density in the inner zone reaches that of the gas density. One would expect that when the grain density exceeds that of the gas, the feedback that the grains impose on the turbulent motions of the gas becomes substantial, and hence the turbulent mixing support of grains should ease off. Presumably a high density core composed of heavy elements is formed at this point (Boss 1998). A special treatment for the inner boundary condition is needed when this happens. We defer a study of the core formation process until a future publication.

4.2.2 Grain growth and vaporisation

We continue to consider only one size for the grains here, but in the interest of adding more realism to our models we allow that size to vary – grow by sticking with other grains, vaporise if gas enveloping the grain is too hot, and limit the grain growth if the differential grain velocity is too large.

Our grain growth model follows the analytical prescription of §3.4, but with the addition of Brownian motions of small grains:

$$\frac{da}{dt} = \left\langle \frac{\rho_g}{4\rho_a}\left(u_{\rm sed} + u_{\rm br}\right) \right\rangle , \quad (82)$$

where $u_{\rm sed}$ is the sedimentation velocity, and $u_{\rm br}$ is the Brownian motion velocity of the smallest grains that dominate grain relative velocities at small values of $u_{\rm sed}$ (Dullemond & Dominik 2005). The Brownian motion velocity is a strong function of the smallest grains size, and we treat it as a free parameter of the model. The signs $\langle$ and $\rangle$ signify grain-mass averaging of the quantities over the first core. This approach is a necessity given that the full radial and particle size distribution function treatment is beyond the scope of our initial study.

Grain fragmentation or cratering may result from grain collisions with inter-grain velocities exceeding a characteristic value, which depends on the size of the grains participating in the interactions (Blum & Wurm 2008). We explore these effects in a very simple fashion, introducing "maximum velocity", $v_{\rm max}$, above which grain growth is significantly reduced compared with equation 82. In particular, we modify the above equation to

$$\frac{da}{dt} = \left\langle \frac{\rho_g}{4\rho_a}\left(u_{\rm sed} + u_{\rm br}\right) \right\rangle \left(\frac{v_{\rm max}}{v_{\rm max} + u_{\rm sed}}\right)^2 . \quad (83)$$

With this prescription, the $da/dt \to 0$ as $u_{\rm sed} \to \infty$.

Finally, the grains are allowed to be vaporised if the gas temperature is large. The vaporisation rate is taken from Helled & Schubert (2008). In practice this prescription implies vaporisation temperature between T = 1200 K and T =1500 K, depending on grain size and relevant time scales. Vaporisation is not important for any models that do not reach 1200 K.

5 NUMERICAL RESULTS

5.1 Constant grain size, no turbulent mixing

We start with the simplest, constant grain size case, setting $a = 10$ cm. We neglect the turbulent grain stirring, i.e., fixing $\alpha_d = 0$. The calculation assumes the grain material density of $\rho_a = 1$ g cm^{-3}, initial mass fraction of $f_g = 0.005$, opacity coefficient $\kappa_0 = 0.01$, opacity power-law index $\alpha = 2$, and the first core's mass of $M_{\rm fc} = 10 M_J$.

Figure 5 presents several snapshots showing the evolution of the gas and the grain components. The snapshots correspond to times $t \approx 360$, 740, 1100 and 1500 years. The first inference from the Figure is that the constant density approximations for the first core itself and for the contracting grain sphere or "cluster" are reasonably good. The analytical estimate of the settling time for this case is $t_{\rm set} = 500$ years (equation 42). Further, equation 56 predicts that the grains will collect into a central sphere the mass density of which equals that of the gas at time $t = 880$ years (for $f_g = 0.005$). In the simulations, this occurs at time almost twice as long. This level of accuracy of the analytical estimates is nevertheless acceptable to us here. The simulations show a somewhat more complex evolution than the simple "top hat" profile.

The upper right panel of the figure shows the radiation flux as a function of radius within the first core. Note that in the last snapshot the heat flux increases significantly in the inner $\sim 10\%$ of the first core. This is a signature of the adiabatic contraction heating imposed by the ever increasing grain density in that region. While until this point the effects of grain sedimentation were hardly felt by the gaseous component anywhere inside the core, the "inverse drag" – grain drag on gas is now significant in the inner region. The gas is however stable against further collapse there as can be seen from velocity curves (lower right panel): the gas and the grain phases continue to separate out, e.g., move with different velocities. The reason for which the gas phase remains gravitationally stable is that it takes a relatively small amount of heating (the bump in the flux curve in the upper right panel) to set up a sufficient pressure gradient to oppose the collapse.

The last snapshot of the figure corresponds to a stage between the grain-dominated one (§3.6.2) and the "bound grain cluster" (§3.6.3). Soon after the last snapshot shown in the figure the grain distribution undergoes a dynamical collapse which we shall study in a future paper.

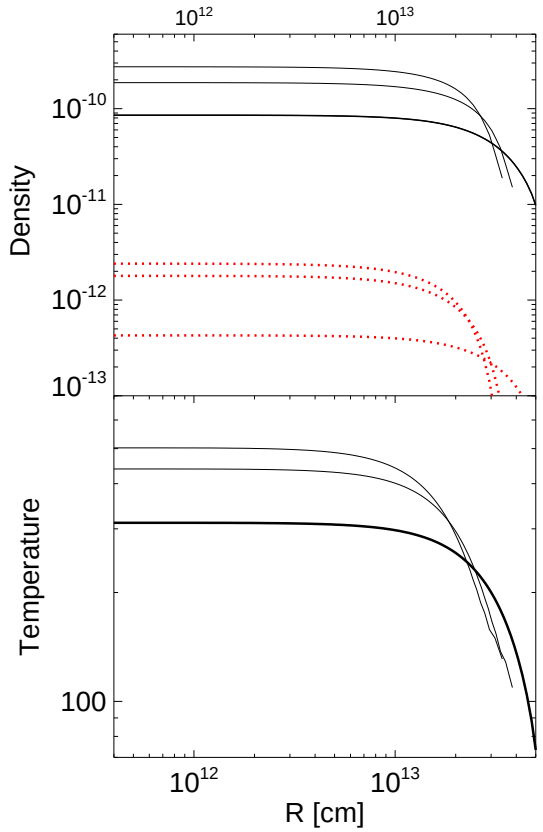

Figure 6. Density (solid for gas, red dotted for grains) and temperature distributions at three different times for the same calculation as in Figure 5, but now with the turbulent mixing coefficient $\alpha_d = 10^{-2}$. The snapshots are for times $t = 0$, 1100 and 2200 years. Note that the grain distribution concentrates towards the centre by a small amount only before coming to an equilibrium in which sedimentation is balanced by turbulent mixing.

5.2 Constant grain size, turbulent mixing

5.2.1 Strong turbulence

We now add turbulent mixing, still keeping the size of the grains constant at $a = 10$ cm. Figure 6 shows the density and temperature distributions for the same case computed in §5.1, but for the turbulent diffusion coefficient $\alpha_d = 0.01$. It is obvious from the snapshot sequence that the dust distribution quickly adjusts to an equilibrium shape in which the rate of gravitational settling is offset by turbulent diffusion. The contraction of the density distribution between the last two snapshots is entirely due to the contraction of the gas distribution, which occurs on the radiative cooling time scale of about 10^4 years. Note that no dense grain cluster forms in this case no matter how long we were to follow the calculation. After the first core has contracted enough to reach $T \sim 2000$ K, it would undergo the well known second collapse (Larson 1969; Masunaga & Inutsuka 2000). Apparently, the effects of grain sedimentation for these particular parameters are completely negligible.

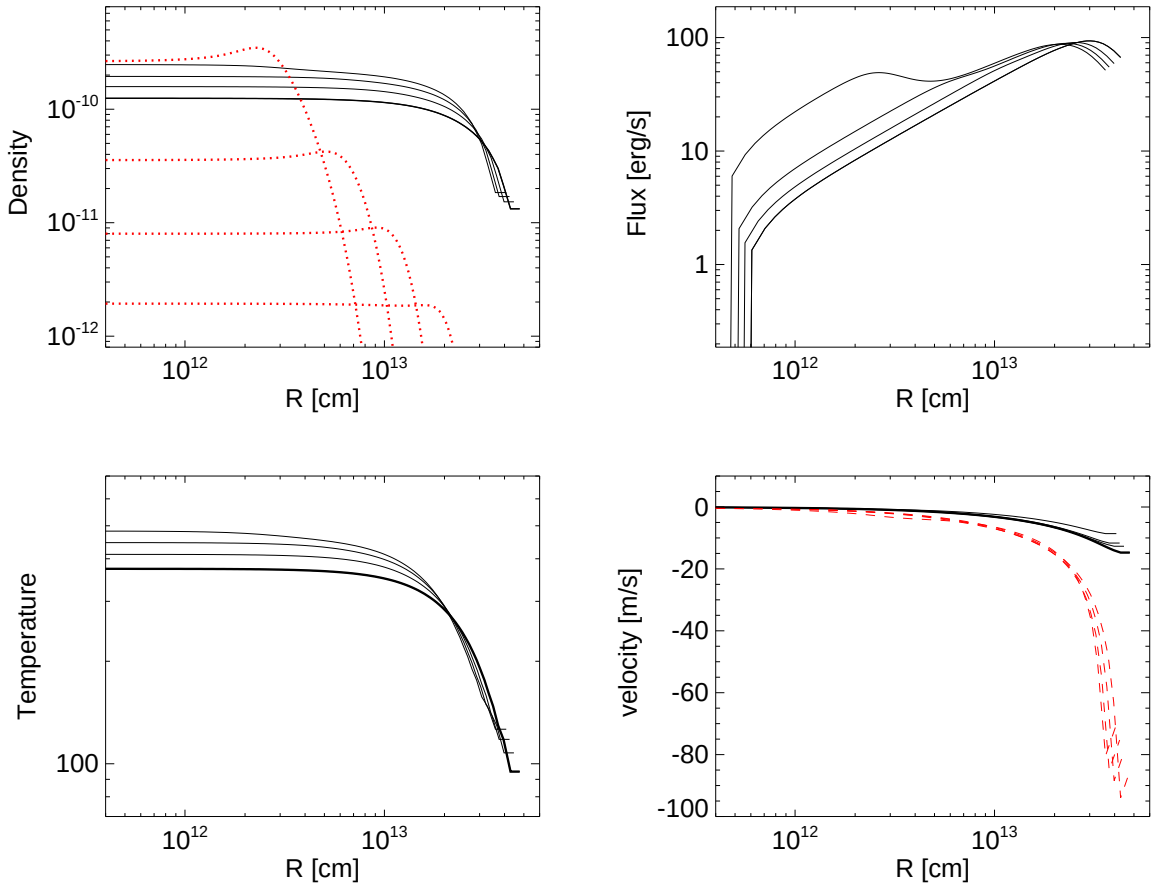

Figure 5. Grain sedimentation for a first core of mass $M_{\rm fc} = 10 M_J$ and a fixed grain size of $a = 10$ cm. The panels show snapshots of gas density, temperature, radiation flux and velocity, as labelled, in solid curves. The dotted and dashed red curves show the grain density and velocity, respectively. The snapshots are for times between $t = 360$ and 1500 years.

5.2.2 Weaker turbulence

Figure 7 shows a calculation identical to that presented in §5.2.1 and in Figure 6, but now for a weaker turbulent mixing, with $\alpha_d = 10^{-3}$. Once again an equilibrium is quickly set up, but a much more concentrated one. It is interesting to note that this equilibrium implies a strong metalicity gradient within the gas cloud, with the most metal rich gas being in the central regions.

5.2.3 Weaker turbulence and larger grains

Our final experiment with fixed size grains is to repeat the calculation of §5.2.2 but with a larger size of grains, $a = 30$ cm. Figure 8 demonstrates a very rapid sedimentation of grains in this case, with gravitational collapse of the "grain cluster" (§3.6.3) occurring by about 500 years. As expected, larger grains are affected significantly less by the turbulent mixing.

The rapid grain sedimentation in this calculation yields a mean grain sedimentation velocity of about 15 m s^{-1} in this model. Such a rapid sedimentation would undoubtedly lead to shattering of some of the grains, so that this calculation is somewhat unrealistic, but it goes to show that if grains can grow to decimetre sizes, then they can probably overcome the effects of turbulent mixing.

5.3 Full models

5.3.1 Simulations Table

We shall now explore our "full" model that includes the grain growth prescriptions (§4.2.2). Selected runs that we performed and discuss below are listed in Table 1. Some of the parameters of the models have very little bearing on the results, except near the boundaries separating qualitatively different regimes. These parameters are not listed in the Table. In particular, the results are insensitive to the initial size of the grain, a_0, and the Brownian motion velocity, $v_{\rm br}$, as long as the latter is large enough (most of the runs were performed with $v_{\rm br} = 5$ cm s^{-1}). This is because, starting from μm-size grains, one finds that grains quickly reach sizes of hundreds of μm anyway (see also more detailed calculations, showing a similar initial rapid grain growth, by Dullemond & Dominik 2005). Thus a_0 is set to 100μm for most tests below.

Given the large differences in the cooling times (§3.1), the form of the opacity law predictably turns out to be quite important. The names for the runs performed with the

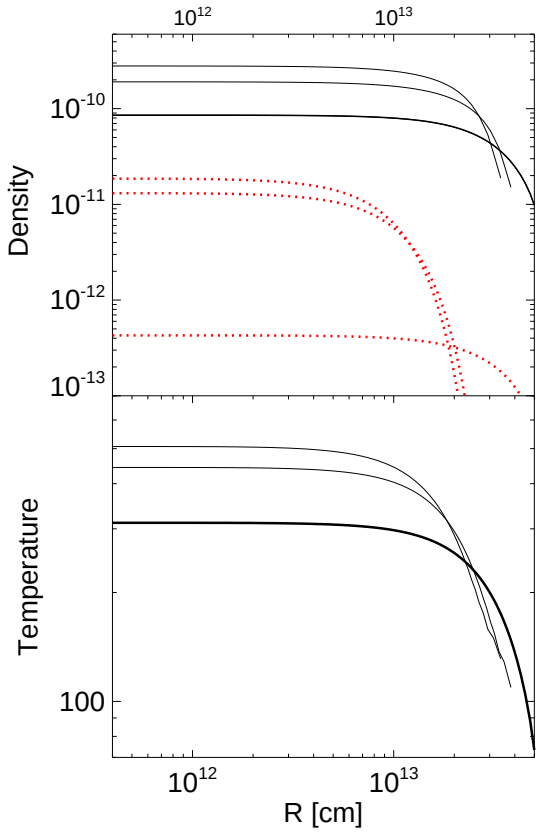

Figure 7. Same as Figure 6, but for a smaller turbulent mixing coefficient, $\alpha_d = 10^{-3}$. The dust is concentrated towards the centre much more than in the previous calculation, but still hovers at an equilibrium state.

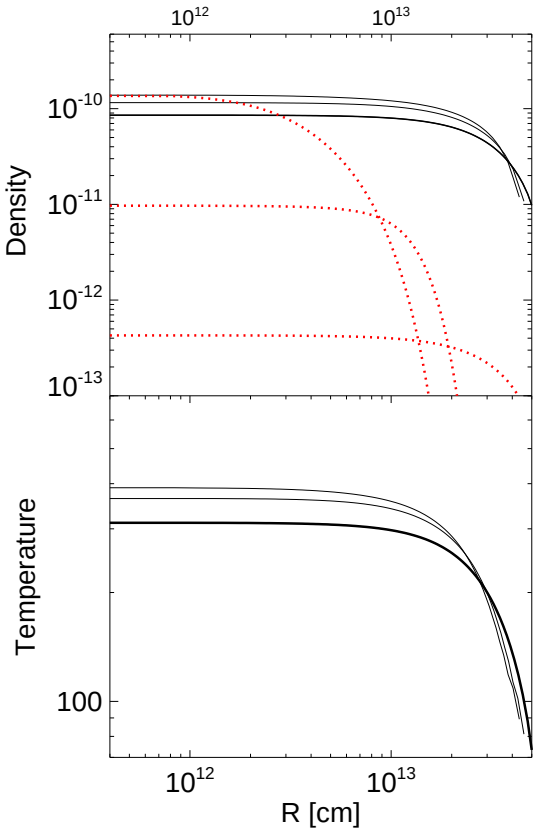

Figure 8. Same as Figure 7, but for larger grains, $a = 30$ cm. The times of snapshots are $t = 0$, 220, and 440 years. Soon thereafter, the inner grain-dominated part of the first core undergoes a gravitational collapse similar to the $\alpha_d = 0$ case studied earlier (Figures 5).

power-law index $\alpha = 1$ starts with a letter "S" for "small opacity", whereas names for $\alpha = 2$ runs start with "L" for "large opacity". These names are not to be taken literally as there is also the opacity coefficient, κ_0, in front of the opacity law we use here (equation 7). κ_0 is also varied in some models.

The last three columns in table 1 list several output quantities of the simulations. $t_{\rm grain}$, T_c and ρ_c are the time at which the self-gravitating phase of the grain sphere evolution is reached (if ever), and the central temperature and the density of gas, respectively, at that time. Grains were vaporised before they could make a massive self-gravitating sphere in the centre in the runs in Table 1 for which no values of these three parameters are given.

5.3.2 Turbulent mixing versus grain growth

We first discuss runs L1, L2 and L3, the three models that are identical to each other except for the value of the turbulent mixing coefficient, which was set to $\alpha_d = 10^{-4}, 10^{-3}$ and 10^{-2}, respectively. There is very little difference in the evolution of the models. This may appear surprising given the all-important role the turbulence played in the simulations with the fixed grain size. The "paradox" is resolved by realising that the runs always start with the turbulence-dominated regime (small grains) and end up in the negligible turbulence one (large grains), and only the time and the boundary between these two vary in L1-L3.

Figure 9 shows the grain size, a, versus time for these three models. The curves are terminated at the point when the central radial bin is dominated by the grains. Initially the curves in the figure are nearly identical to each other. This can be understood by realising that at a small a, sedimentation speeds are low, so that turbulent mixing easily balances sedimentation. A quasi-steady state results in which grain sedimentation is neutralised by turbulent mixing.

Figure 9 shows that grain growth is slightly faster for higher levels of turbulence. We explain it by the fact that the grain distribution is slightly more extended in this case, hence the sedimentation velocity, proportional to R (see equation 41), is larger, allowing the grains to sweep up smaller ones at a faster rate and hence grow faster.

The process of grain growth accelerates with time. At early times this is due to the fact that $u_{\rm sed} \propto a$, thus $da/dt \propto a$ (see equation 82). At later times, grains become over-abundant in the inner regions, i.e., $\rho_g/\rho > f_g$ there. This speeds up the rate at which the larger grains can sweep up the smaller grains even further. This non-linear stage of grain growth is naturally reached faster by the lower turbu-

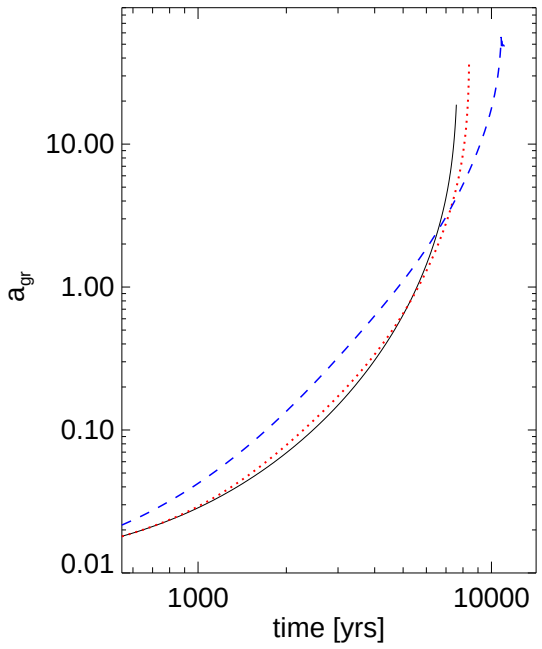

Figure 9. Grain size versus time for models described in §5.3. The solid black, the red dotted and the blue dashed curves are for $\alpha_d = 10^{-4}, 10^{-3}$ and 10^{-2}, respectively.

lence models. A corollary of this is that the higher turbulence runs reach the grain self-gravitating phase with higher temperature and density.

Nevertheless, it is notable how qualitatively similar the three simulations actually are. One difference is the time when the central region becomes grain-dominated. It is $t =$ 7.6, 8.4 and 11 thousand years for $\alpha_d = 10^{-4}, 10^{-3}$ and 10^{-2}, respectively. The later the grain-dominated phase reached, the hotter is the central region of the first core, and the denser it is (see Table 1).

The main conclusion we can draw from these experiments is that the turbulent diffusion is only likely to delay rather than stop grain sedimentation *if* grain growth can proceed via the hit-and-stick process faster than the gas heats up to vaporise the grains.

5.3.3 Delayed sedimentation due to grain fragmentation

To explore sensitivity of our grain growth model to grain fragmentation due to high speed collisions, we ran several models where the maximum velocity parameter $v_{\rm max}$ was reduced from the nominal value of 10 m s^{-1} to 1 m s^{-1} (see Table 1). In particular, simulation L2a is identical to L2 except for the smaller value of $v_{\rm max}$. Qualitatively the two runs are similar, but the grain-dominated cluster phase is reached at time almost twice as long in L2a than in L2. This is caused by the subdued grain growth rate in the run L2a compared with L2.

Concluding, as envisaged earlier in §3.8, grain sedimentation may still proceed reasonably quickly at realistically small ($\sim$m s^{-1}) values of $v_{\rm max}$.

5.4 Vaporisation of grains in rapidly cooling first cores

In the context of our model of isolated first cores, the only robust way to stop grain sedimentation is to prevent their growth. This occurs when the first cores become too hot, so that grains vaporise. We find this behaviour if (a) the cores are too hot (too massive) to begin with; (b) the opacity is low so that the cores cool very quickly (thus leading to hotter internal temperatures); (c) the grain content of the core is low, yielding too long grain growth times.

Figure 10 shows the grain size and temperature as a function of time for three runs that yielded no grain sedimentation. The solid black curve is the simulation S3 (cf. Table 1) – a low opacity, $\kappa_0 = 0.001$, and low grain mass fraction case, $f_g = 1.2 \times 10^{-3}$, with the first core mass of $M_{\rm fc} = 5M_J$. The opacity law exponent is $\alpha = 1$. Both conditions (b) and (c) are the case for this particular run. The grains manage to reach the size of about 1 cm before they are vaporised. The central gas temperature is almost 1400 K at that time. Grain vaporisation actually starts earlier, at $T_c \sim 1300$ K or so, but does not immediately prevail over the process of grain growth.

The other two runs shown in figure 10 have much more massive cores, $M_{\rm fc} = 25M_J$ (S7 in Table 1; dotted red curve) and $M_{\rm fc} = 20M_J$ (S6; dashed blue). The opacity coefficient $k_0 = 0.05$ and 0.01, for the runs, respectively, and the grain mass fraction is $f_g = 0.01$ for both. The cores cool quickly nevertheless as the opacity power law index $\alpha = 1$, hence the short cooling times (equation 21). The most massive first core considered here (blue curve) is almost too hot to allow grain growth to begin with (case "a" above). As the cooling time is short, the core undergoes a quick and nearly dynamical evolution in the beginning, driving hydrodynamical oscillations that allow some early grain growth. However the latter is quickly turned into grain evaporation as the core settles into its cooling evolution.

5.5 Importance of grain fraction (metalicity)

Amongst the parameters of the simulations that we varied is the first core's initial grain mass fraction, f_g (Table 1). A higher grain content obviously favors grain growth. For example, the runs L4 and L5 are identical except for the grain mass fraction, $f_g = 0.005$ and 0.02, respectively. Not surprisingly, the grain-dominated phase is reached far faster in L5 than in L2. Therefore, we can expect that metalicity of the first core is one of a key parameters determining whether grain sedimentation takes place or not.

6 DISCUSSION

6.1 Summary of the results

In this paper we explored the possibility that grains may sediment inside isolated or slowly accreting first cores, which are the gaseous condensations with mass between about 5 and 50 Jupiter masses. While many parameters (such as the turbulent viscosity parameter) determine the end result, the main requirement for sedimentation to take place is a rapid enough grain growth. Based on numerical experiments, sedimentation occurs as long as grains can grow to a few

Table 1. Parameters of the simulations. The mass of the first core, $M_{\rm fc}$, is in Jupiter's masses; k_0 is the opacity coefficient in the opacity law given by equation 7; α is the power law index in that law; f_g is the grain mass fraction of the core; α_d is the turbulent mixing coefficient; $v_{\rm max}$ [m s^{-1}], the maximum velocity before grain-grain collisions stifle grain growth (equation 82); $t_{\rm grain}$ is the time at which the innermost gaseous cell becomes dominated by grains, by mass, in units of 10^3 yrs; and $T_{\rm c}$ and $\rho_{\rm c}$ are the gas temperature and density there at the time, in cgs units.

ID	$M_{\rm fc}$	k_0	α	f_g	α_d	$v_{\rm max}$	$t_{\rm grain}$ (10^3 yrs)	$T_{\rm c}$	$\rho_{\rm c}$
S1	10	0.01	1	0.005	5×10^{-2}	10	2.7	1400	1.4×10^{-8}
S2	10	0.001	1	0.005	5×10^{-2}	–	–	–	
S3	5	0.001	1	0.0012	10^{-3}	1	–	–	–
S4	5	0.003	1	0.0012	10^{-3}	1	3.3	1270	1.5×10^{-8}
S6	20	0.01	1	0.02	10^{-3}	1	–	–	–
S7	25	0.05	1	0.02	10^{-3}	1	–	–	–
L1	10	0.01	2	0.005	10^{-4}	10	7.8	695	7.5×10^{-10}
L2	10	0.01	2	0.005	10^{-3}	10	8.4	710	8×10^{-10}
L3	10	0.01	2	0.005	10^{-2}	10	11.0	750	10^{-9}
L2a	10	0.01	2	0.005	10^{-3}	1	13.4	790	1.2×10^{-9}
L4	10	0.001	2	0.005	5×10^{-2}	10	1.9	1190	4×10^{-9}
L5	10	0.001	2	0.02	5×10^{-2}	10	0.69	1130	3×10^{-9}
L6	10	0.1	2	0.005	10^{-3}	10	16.0	360	1.3×10^{-10}
L7	40	0.1	2	0.005	10^{-3}	10	15.3	1100	2.1×10^{-10}
L8	55	0.1	2	0.005	10^{-3}	10	–	–	–

cm to a few tens of cm before vaporisation temperature of $T\approx1400$ K is reached. This is expressed mathematically as

$$t_{\rm gr} < t_{\rm vap}\ , \tag{84}$$

where $t_{\rm gr}$ is the grain growth time scale (equation 49), and $t_{\rm vap}$ is the vaporisation time of the grains (equation 33). Turbulent mixing and grain shattering by collisions may slow down grain growth compared with the analytical model (in which case $t_{\rm gr}$ must be obtained numerically).

While the outcome depends on several parameters – mass of the first core, $M_{\rm fc}$, ambient gas temperature, $T_{\rm init}$, opacity law in the first core, the initial grain mass fraction, f_g, turbulent mixing, etc., we shall here give only one example of the implications of the equation 84. In particular, we shall fix $f_g=0.005$, $\alpha_d=10^{-3}$, $v_{\rm max}=10$ m s^{-1}, and $T_{\rm init}=10$ K.

With these parameters fixed, we can ask the following question: At a given opacity coefficient κ_0, what is the range of the first core masses that could support the dust sedimentation?

Figure 11 answers this question for the two opacity power-law indexes that we studied here, $\alpha=1$ (black dotted curve) and $\alpha=2$ (red dashed one). The lower (solid) line gives the minimum mass of the first core which we obtained by requiring that the mean first core density (equation 11) is at least equal that at which the collapsing gas switches to the adiabatic behaviour (equation 8). This curve is independent of α for $T_1=1$. The curves dividing the parameter space are obtained by solving the equation 84 with our analytical model for grain growth and the first core contraction. The asterisks are the maximum first core mass for which grain sedimentation occurs found numerically for the $\alpha=2$ case. They are encouragingly close to the analytical curve. The fact that they are slightly below is probably explained by the extra delay in the grain growth that the turbulent mixing and the maximum velocity $v_{\rm max}$ impose in numerical simulations compared with the analytical models that do not account for these processes.

This limited survey of parameter space demonstrates that there range in $M_{\rm fc}$ in which grain sedimentation is possible is about a factor of 10 wide for $\alpha=2$, and shifts to higher masses for higher opacities. This is to be expected, as higher opacity implies longer cooling times.

The $\alpha=1$ case (black dotted line) shows a narrower window of opportunity for dust sedimentation, which is again a cooling effect. As these cores cool quicker, there is less time for dust growth.

6.2 Comparison to previous work

Our analytical model and numerical simulations confirm the suggestion made by Boss (1998) that grains can grow and sediment inside giant embryo, although started from a much less dense initial configuration. While a fuller comparison is to be made in paper II where we continue the calculations to the point of the solid core formation, we can already see that this lower density and temperature initial configuration is key to address the criticism levelled on the Boss (1998) model by Wuchterl et al. (2000), later confirmed by Helled et al. (2008); Helled & Schubert (2008). These au-

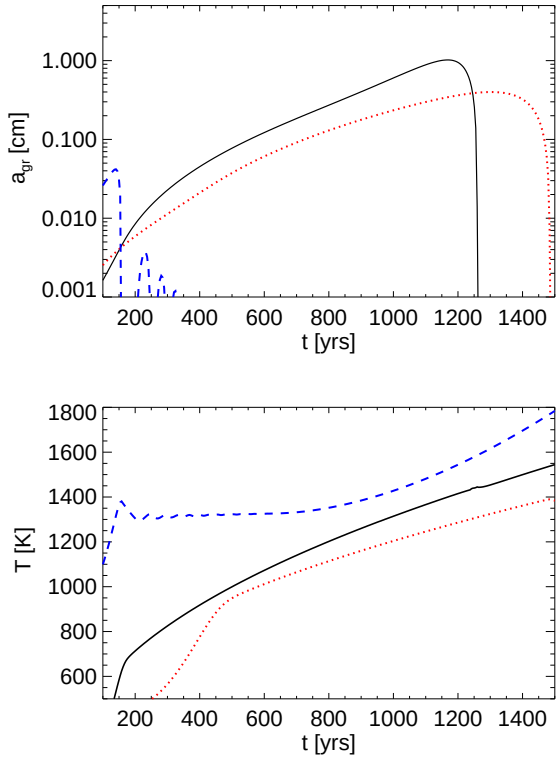

Figure 10. Grain size versus time (upper panel) and the central gas temperature (lower panel) for three cases that led to grain vaporisation rather than growth: S3 (solid black), S6 (dashed blue) and S7 (red dotted). In all three cases the first core cools radiatively, contracts, and becomes too hot to allow grain growth.

thors found that their giant planet models were convective, and that convective grain mixing has significantly slowed down the core growth.

Since the initial column depth of the embryos is much lower in our models, the radiative cooling remains strongly dominant over convective cooling for $\sim 10^4 - 10^5$ years, the time it takes (see figure 2) for the embryos to contract to densities and temperatures considered by the authors mentioned above. These findings echo the results by Bodenheimer (1974) who studied early contraction of a 1 Jupiter mass gas cloud and concluded that the planet remained radiative during the first $\sim 10^5$ years. While his model does not include dust sedimentation, it accounts for H_2 molecules dissasociation, hydrogen ionisation, and much more (that we do not include here). His calculations also used similarly cool initial conditions (43 K was the initial temperature of his model planet).

Therefore it appears that most of the differences between us and Helled et al. (2008); Helled & Schubert (2008) can be traced to the significantly different initial conditions. In terms of applications to planet formation field, the differences in our results and that of Helled et al. (2008); Helled & Schubert (2008) are striking. These authors found that a 5 Jupiter mass embryo cannot yield any dust sedimentation as it is too hot to begin with, e.g., the initial temperature above the grain vaporisation temperature. In contrast, we find that a 5 Jupiter mass embryo provides an excellent environment for dust growth: the gas temperature is initially less than 100 K and stays below 1400 K for as long as 10^4 to more than 10^5 years, depending on the opacity (cf. figure 1).

In paper II we do find that convection becomes very important in the inner region of the embryo *once a massive solid core forms*, as this releases a significant amount of heat. It is also interesting to note that while our initial condition is significantly different, the inferred grain growth and sedimentation time scales are from 10^3 to 10^4 years, in a broad agreement with the estimate by Boss (1998).

On the other hand, in a qualitative agreement with Helled et al. (2008); Helled & Schubert (2008), the conditions for dust growth found to deteriorate with an increasing mass of the gas clumps. Depending on opacity, grains cannot sediment for giant embryo masses higher than ~ 10 to a few tens Jupiter masses.

6.3 Astrophysical implications

Our calculations here and in paper II lend support to the ideas presented by Boss (1998), except that grain sedimentation process must start earlier in the life of the protoplanet, while it can still be considered the first core. Lower initial temperatures and rather long cooling times of the giant embryo in the latter stage are key for a successful grain sedimentation outcome.

Boss et al. (2002) argued that giant embryos may yield not only giant planets but also giant icy planets with cores if the metal poor envelopes of the embryos are removed. Irradiation by a nearby star was suggested to accomplish this. While this is certainly possible, it may be not very probable as OB stars are rare.

The present paper is the base for paper III, where we argue that giant embryos may migrate inward due to the gravitational torques from the disc. Estimates show that embryos may migrate to the distance of several AU to the parent star in several $\times 10^4$ years, typically. As cooling of embryos slows down as they age, the embryos must be eventually disrupted by the tidal forces or by the heating due to irradiation from the parent star. This opens up an exciting possibility that *all* planets may be formed by such a modified version of gravitational instability model.

7 CONCLUSIONS

In this paper we considered the grain growth and sedimentation process inside the giant planet embryos, which we argued must be nearly identical in properties to the first cores. These are the first gaseous hydrostatic condensations from which stars may form. We found that grains can indeed grow and sediment to the centre of the gas cloud provided that the gas remains cool enough (temperature below ~ 1400 K) for the time it takes the grains to reach a few cm size. The efficiency of the dust sedimentation process and the final mass of the solid core are strong functions of opacity and other parameters of the problem.

We suggested that astrophysical applications of these results may be in the field of planet formation, where giant planet embryos may serve as birth places for all types of planets if these embryos migrate inward and get tidally or

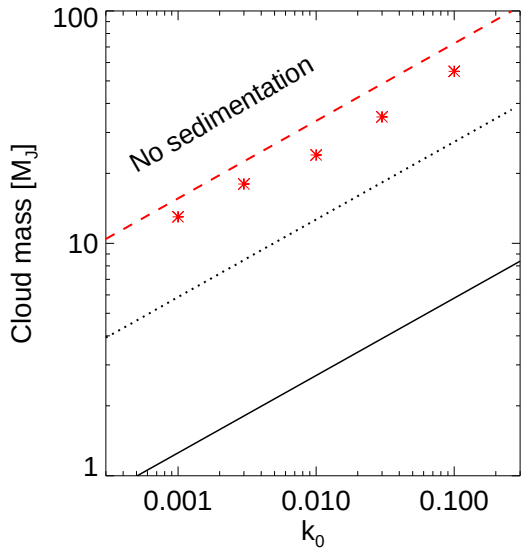

Figure 11. Minimum first core mass (solid curve) and maximum first core mass for grain sedimentation versus the opacity coefficient κ_0 for $\alpha = 1$ (black dotted line) and $\alpha = 2$ (red dashed line). No grain sedimentation is expected above these lines as grains get vaporised faster than they can sediment. See text for further detail.

irradiatively disrupted in the inner few AU from the parent star.

8 ACKNOWLEDGMENTS

The author is indebted to Richard Alexander and Seung-Hoon Cha for useful discussions of the problem, and to Roman Rafikov and Phil Armitage for comments on the draft. Comments by the anonymous referee were instrumental in improving the clarity and astrophysical relevance of the paper. Theoretical astrophysics research at the University of Leicester is supported by a STFC Rolling grant.

REFERENCES

Bate M. R., Bonnell I. A., Bromm V., 2003, MNRAS, 339, 577
Blum J., Wurm G., 2008, ARA&A, 46, 21
Bodenheimer P., 1974, Icarus, 23, 319
Bodenheimer P., Laughlin G. P., Rózyczka M., Yorke H. W., eds., 2007, Numerical Methods in Astrophysics: An Introduction
Boss A. P., 1997, Science, 276, 1836
Boss A. P., 1998, ApJ, 503, 923
Boss A. P., Wetherill G. W., Haghighipour N., 2002, Icarus, 156, 291
Dullemond C. P., Dominik C., 2005, A&A, 434, 971
Fortney J. J., Nettelmann N., 2009, Space Science Reviews, 115–+
Fromang S., Papaloizou J., 2006, A&A, 452, 751
Gammie C. F., 2001, ApJ, 553, 174
Garaud P., Lin D. N. C., 2004, ApJ, 608, 1050
Helled R., Podolak M., Kovetz A., 2008, Icarus, 195, 863
Helled R., Schubert G., 2008, Icarus, 198, 156
Larson R. B., 1969, MNRAS, 145, 271
Low C., Lynden-Bell D., 1976, MNRAS, 176, 367
Lubow S. H., Seibert M., Artymowicz P., 1999, ApJ, 526, 1001
Masunaga H., Inutsuka S., 1999, ApJ, 510, 822
Masunaga H., Inutsuka S.-i., 2000, ApJ, 531, 350
Masunaga H., Miyama S. M., Inutsuka S.-I., 1998, ApJ, 495, 346
Meru F., Bate M. R., 2010, ArXiv e-prints
Rafikov R. R., 2005, ApJL, 621, L69
Rees M. J., 1976, MNRAS, 176, 483
Rice W. K. M., Lodato G., Armitage P. J., 2005, MNRAS, 364, L56
Safronov V. S., 1969, Evoliutsiia doplanetnogo oblaka.
Shakura N. I., Sunyaev R. A., 1973, A&A, 24, 337
Stamatellos D., Whitworth A. P., 2008, A&A, 480, 879
Toomre A., 1964, ApJ, 139, 1217
Weidenschilling S. J., 1977, MNRAS, 180, 57
Weidenschilling S. J., 1980, Icarus, 44, 172
Wetherill G. W., 1990, Annual Review of Earth and Planetary Sciences, 18, 205
Wuchterl G., Guillot T., Lissauer J. J., 2000, Protostars and Planets IV, 1081–+